JIMMA UNIVERSITY

COLLEGE OF NATURAL SCIENCES

DEPARTMENT OF CHEMISTRY

M.Sc THESIS

SYNTHESIS OF ZnO AND Cu-DOPED ZnO NANOPARTICLES USING *ALOE VERA* LEAF EXTRACTS AND EVALUATION OF THEIR ANTIBACTERIAL AND PHOTOCATALYTIC ACTIVITIES

BY: MULATU DEGEFA

ADVISOR: GUTA GONFA (Ph.D)

CO- ADVISOR KIRUBEL TESHOME (Ass.Prof)

NOVEMBER, 2021

JIMMA, ETHIOPIA

SYNTHESIS OF ZnO AND Cu-DOPED ZnO NANOPARTICLES USING *ALOE VERA* LEAF EXTRACTS AND EVALUATION OF THEIR ANTIBACTERIAL AND PHOTOCATALYTIC ACTIVITIES

THIS THESIS IS SUBMITTED TO THE SCHOOL OF GRADUATE STUDIES JIMMA UNIVERSITY IN PARTIAL FULFILMENT OF THE REQUIREMENTS FOR THE DEGREE OF MASTER OF SCIENCE IN INORGANIC CHEMISTRY.

ADVISOR'S APPROVAL SHEET

To: Chemistry Department

Subject: Thesis Submission

This is to certify that the thesis entitled "**Synthesis of ZnO and Cu-doped ZnO Nanoparticles using *Aloe Vera* leaf extracts and evaluation of their antibacterial and photocatalytic activities**" submitted in partial fulfillment of the requirements for the degree of Master of Science in inorganic Chemistry. The Graduate program of the department of Chemistry, and has been carried out by Mulatu Degefa under our supervision. Therefore, we recommend that the student has fulfilled the requirements and hence hereby he can submit the thesis to the department.

Name of Advisor	Signature	Date
Guta Gonfa (Ph.D)	_____	_____

Name of Co-Advisor	Signature	Date
Kirubel Teshome (Ass.Prof**)**	_____	_____

DECLARATION

I hereby declare that this M.Sc Thesis is my original work and has not been presented for a degree in any other university, and all sources of material used for this thesis have been duly acknowledged.

Name: Mulatu Degefa

Signature: _____

This M.Sc thesis has been submitted for examination with our approval as thesis advisors.

Advisor Name: Guta Gonfa (Ph.D) Co-Advisor Name: Kirubel Teshome (Ass. Prof)

Signature: _____ Signature: _____

Date of submission: _____

APPROVAL OF BOARD OF EXAMINER

Advisor	signature	Date
_____	_____	_____
Co-Advisor	signature	Date
_____	_____	_____
Internal Examiner	signature	Date
_____	_____	_____
External Examiner	Signature	Date
_____	_____	_____
Chairperson	signature	Date
_____	_____	_____

ACKNOWLEDGEMENTS

First I would like to thank the almighty God who gave me the strength and wisdom to complete my work successfully.

Next, I would like to express my genuine heartfelt gratitude to my advisor, Dr. Guta Gonfa for his priceless suggestion, comments, corrections, professional, guidance, and friendly approach throughout my work for the successful accomplishment of this thesis.

I would also like to express my deepest gratitude to my Co-adviser, Mr.Kirubel Teshome for his patience, fruitful advice and friendly approach throughout my work.

I would like to express my very great appreciation to the Department of Chemistry, Jimma University for giving great opportunity to study my M.Sc in inorganic chemistry.

My acknowledgement is also extended to Oromia environmental protection, forest, and climate change authority for allowing me to join this postgraduate program and sponsorship of my study.

Finally, my cheerful thanks go to my wife Atsade Negash, my family members, and all my colleagues who give me moral during my study.

TABLE CONTENT

Contents **page**

LIST OF ABBREVIATIONS

Cu-doped ZnO NPs	Copper- doped zinc oxide nanoparticles
Cu	Copper
CB	Conduction band
DI	Deionized water
Eg	Energy band gap
eV	Electron Volt
E.coli	Escherichia Coli
S.aureus	Staphylococcus aureus
FT-IR	Fourier transforms infrared
FWHM	Full Width at Half Maximum
KBr	Potassium Bromide
JCPDS	Joint Committee on Powder Diffraction Standards
LED	Light Emitting Diodes
MB	Methyl blue
MHA	Muller Hinton Agar
nm	Nanometer
NPs	Nanoparticles
ppm	Parts per million
PDE	Percentage degradation efficiency
PZC	Point of zero charge
Rpm	Revolutions per minute
ROS	Reactive Oxygen Species
SEM	Scanning electron microscope
SPR	Surface Plasmon resonance
UV-Vis	Ultraviolet-visible
VB	Valance band
XRD	X-ray diffraction
ZnO-NPS	Zinc oxide nanoparticles

LIST OF FIGURES

LIST OF TABLES

LIST OF APPENDICES

ABSTRACT

In recent years, nanoparticles synthesis by biological method has gained extensive attention due to its low cost, simplicity, non-toxic and environmentally-friendly nature, compared with chemical and physical synthesis methods. The aim of this study is to fabricate *Aloe vera* leaf extract supported ZnO and Cu-doped ZnO nanoparticles for their photocatalytic and antibacterial activities evaluation. ZnO and Cu-doped ZnO nanoparticles were prepared from zinc nitrate hexahydrate and copper nitrate trihydrate using the plant extract. The synthesized nanoparticles were characterized by using UV-Vis, FT-IR, XRD, and SEM spectroscopic techniques, and tested as antibacterial and photocatalysts. The UV-Visible spectra showed absorbance peaks at 358 nm, 365 nm, and 379 nm, which correspond to the characteristic band of ZnO, 1% Cu-doped ZnO, and 4 % Cu-doped ZnO nanoparticles respectively. FT-IR confirmed the nature of bonds and functional groups in the leaf extract, ZnO and Cu-doped nanoparticles. The XRD analysis reveals all the synthesized particles have a crystalline nature with a particle size of 19.24 nm, 23.74 nm, and 24.91 nm of ZnO, 1% Cu-doped ZnO and 4% Cu-doped ZnO NPs respectively. SEM image showed irregular, crushed-ice, and spherical shapes of the NPs. The antibacterial activity studies of the synthesized 1% Cu- doped ZnO and 4 % Cu-doped ZnO Nps against *Staphylococcus aureus, Bacillus cereus, Escherichia. Coli* and *salmonella typhi* showed good potential with the reference to the selected standards Gentamicin and DMSO. The maximum zone inhibition activities were found against gram-positive (*B. cereus and S. aureus*) for 4% Cu-doped ZnO NPs followed by 1% Cu-doped ZnO NPs, whereas minimum inhibition zone were seen against gram-negative (*E.coli and S.typhi*). 1% Cu-doped ZnO and 4% Cu-doped ZnO NPs displayed good degradation efficiency, 78.48% and 88.07% respectively after 180 min of irradiation, 4% Cu-doped ZnO NPs showing better photocatalytic efficiency.

Keywords:- Zinc oxide nanoparticles, *Aloe Vera*, Green synthesis, Antibacterial Activities, Photocatalytic Activities, Methylene Blue

.

1. INTRODUCTION

1.1. Background of the study

Water pollution by dyes is a worldwide problem particularly in the textile industry where large quantities of dye effluents are discharged from the dyeing process. Wastewater has been found to contain dyes from different industries which are potentially risky to human health. The production of these dyes and pigments is more than 7 $x10^5$ tons and approximately 5 - 15 % is lost in the industrial effluents [1]. Effluents contaminated with dyes that are discharged into oceans, seas, rivers and ponds from textile factories and the like can bring disturbance to the water eco-system due to toxic properties of the dyes and blockage of sun light to reach the plankton in the water system [2] (Figure 1). Various organic pollutants like methyl orange, methylene blue, Congo red, and methyl violet are discharged to water from industries. Methylene blue ($C_{16}H_{18}N_3SCl$) is commonly used as a representative of widespread organic dyes that contaminate textile effluents and that are lowering light penetration, photosynthesis and damage the aesthetic nature of the water surface [3].

Deep colored methylene blue (MB) dye is discharged widely in wastewater and the existence of MB in water can cause irritation on the eye, nausea, vomiting and diarrhea when in contact or when taken orally by humans. It is not easy to remove from wastewater owing to their stability to oxidizing agents, they also undergo a slow or incomplete degradation process hence generates some environmental problems [4].

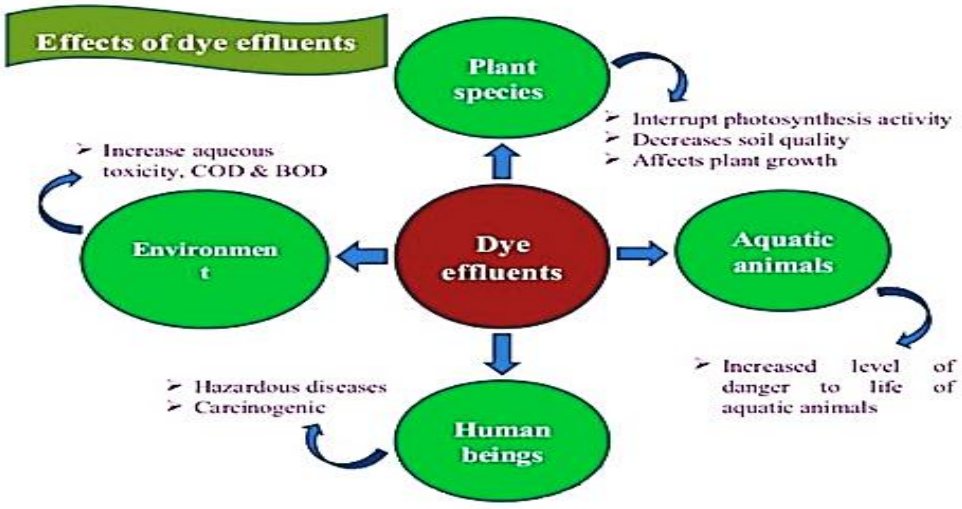

Figure 1 :Effect of textile dye effluent on environment [5]

Different Conventional methods, like flocculation, coagulation, [5] filtration, and precipitation, have been used to remove pollutants. However, each treatment methods generate another problem due to a low efficiency [6] in terms of feasibility, reliability, environmental impact, pre-treatment requirements, and the formation of potentially toxic by-products. Among other methods, advanced oxidative processes (AOPs) which include photocatalysis, has been used in the destruction of organic contaminants [7]. Photocatalytic degradation (combination of a semi-conductor and UV light) method is being given more attention because of its efficiency, versatility, convenience, ease of the process, low cost, an environmentally clean process for treatment of pollutants. Another advantage of photocatalysis is its ability to break down pollutants into less toxic compounds such as CO_2 and H_2O [8]. The photocatalytic materials have also shown antibacterial properties which compete with multidrug-resistant pathogens like *E. coli*, *S. aureus*, *P. aeroginosa*, *S. mutans*, etc.[9].

In the modern research era, nanoscience, as well as nanotechnology, are widely applied in different fields such as sensor, electronic, antibacterial, water purification, cosmetic, biomedical, pharmaceutical, environmental, catalytic, and material applications [10]. Transition metal oxides with nanostructure and semiconductors with dimensions in the nanometer real have attracted considerable interest in many areas of chemistry, physics, material science, biotechnology, information technology and environmental technology as next generation technologies [11].

The size, crystallinity, and morphology of nonmaterials can greatly influence their catalytic, magnetic, electronic and optical properties [12]. In recent times, the synthesis of metal and metal oxides (like Ag, TiO_2, MgO, CuO, and ZnO) has drawn special attention, considering their bactericidal and bacteriostatic possible applications in the field of Nanomedicine. Among these metal oxides, zinc oxide nanoparticles (ZnO NPs) are quite unique and have been acknowledged as a promising alternative photocatalyst due to their non-toxicity, high catalytic capability, and cost-effectiveness [13]. Prototype ZnO NPs have been used as delivery systems for vaccine and anticancer drugs. However, ZnO has a wide direct band gap of 3.37 eV and a substantial exciton binding energy of 60 meV [14]. Therefore, ZnO photocatalytic activities are activated upon illumination with a UV radiation source. It has been established that ultraviolet and visible light constitute 5–7% and 46% of solar energy, respectively [15] Thus, it is more economical to develop a visible light-activated photocatalyst for bacteria disinfection in surfaces, water, and air.

Often, doping of ZnO with impurity is usually targeted at introducing intra-band gap energy levels that allow ZnO to utilize visible light for photocatalytic application. Presently, there is so much attention given to the alteration of ZnO NPs by doping it with transition metals like Ag, Co, Fe, Ni, and Mn to improve its spectral sensitivity [16]. These studies have demonstrated that transition metals as dopants can affect the grain size of ZnO NPs together with their optical properties. Copper is selected as a dopant in this work because it has high electronic conductivity and availability, relatively cheap [17] and their ionic radii is nearest to similar which is 0.73 for Cu and 0.74 for Zn. When ZnO is doped with Cu, the biological and photocatalytic activities become enhanced due to surface area enhancement.

Chemical, physical, and biological approaches have been used to synthesize NPs [18]. However, biological synthesis of NPs has become one of the most preferred methods simply because it is eco-friendly. Biosynthesized ZnO NPs have been shown to be bio-safe, biocompatible, and desirable for medical applications like drug carriers, cosmetics, and the coating of medical materials [19]. Consequently, attention is directed towards plants that are used for the synthesis of NPs because they contain most of the bioactive compounds that can reduce metal salts to metal nanoparticles [20]. *Aloe vera* is a shrubby, perennial succulent plant of the Liliaceae family having flavonoids, saponins, and alkaloids [21]. Currently, there were literatures reported on plant extracting supported ZnO and a few literatures reported on plant extract supported Cu-doped ZnO nanoparticles for antibacterial activity and photodegradation. However, there is no report on the synthesis of *Aloe vera* supported Cu- doped ZnO NPs for degradation of methylene blue and antibacterial activities.

Hence, we reported synthesis of ZnO and Cu-doped ZnO NPs, with their antibacterial activities against gram-positive bacteria (*Bacillus cereus* and *Staphylococcus aureus)* and gram-negative bacteria (*Escherichia coli and Salmonella typhi).* Furthermore, the photocatalytic activities were investigated using methylene blue (MB) as the test contaminant.

1.2. Statements of the problem

Many countries in the world have been moving forward with increasing population and advanced technologies, but distressing with serious problems such as environmental pollution caused by the textile industry, colored dyestuff result water contamination, which are causing human and animal health problems. Among the major sources, organic industrial effluents like Methylene

blue have been widely used in textile industries. On the other hand, emerging infectious diseases and the development of drug resistant bacteria at an alarming rate is a matter of serious concern and an increasing public health problem. These infections are caused by various pathogens, most of which are resistant to traditional and conventional methods of treatment. New strategies for controlling water contamination and bacterial activities are urgently needed and nanomaterials emerging as a promising candidates. Nanoparticles synthesis using a green synthetic method employing plant extracts is one of the more extensively acknowledged approach due to its several advantages, such as require no additional chemicals, simplicity, environmentally friendly, and inexpensiveness [22]. Nanoparticles synthesized by this approach are showing good antibacterial and photocatalytic dye degradation activities. Thus, the present study is intended to evaluate the photocatalytic dye degradation, and antibacterial activities of ZnO and Cu-doped ZnO NPs synthesized using *Aloe vera* leaf extract, with answering the following research questions.

1. Do phytochemicals present in *Aloe vera* leaf extract act as a good stabilizing and capping agent for the ZnO and Cu-doped ZnO NPs formation?
2. Do the synthesized ZnO and Cu-doped ZnO NPs have potential for photocatalytic and antibacterial activities?

1.3. Objectives of the study

1.3.1. General Objective

To synthesize ZnO and Cu-doped ZnO nanoparticles using *Aloe Vera* leaf extracts for evaluation of their antibacterial and photocatalytic activities.

1.3.2. Specific objectives

- To prepare *Aloe vera* leaf extract.
- To synthesize ZnO and Cu-doped ZnO nanoparticles using *Aloe vera* leaf extract.
- To characterize the synthesized nanoparticles using UV-Vis, XRD, FT-IR, and SEM spectroscopic techniques.
- To evaluate photocatalytic and antibacterial activities of ZnO and Cu-doped ZnO nanoparticles.

1.4. Significance of the study

Today, major industries are using a high volume of water and produce a large number of effluents containing a large amount of wastewater flowing from dyeing and finishing processes, which cause environmental pollution and affect human health. As a result, synthesis of ZnO and Cu-doped ZnO NPs by green approach encompass various significances. In different field of studies, it may contribute for the search of potential nano based antibiotic drugs and also reduces toxicity due to various contaminants released to the environment.

2. REVIEW OF RELATED LITERATURES

2.1. Over View of Nanoparticles, Nanotechnology and Nanoscience

Nanoparticles are of scientific interest as they are, in effect, a bridge between bulk materials and atomic or molecular structures. It is referred to the length scale of one billionth of a meter. Thus, nanoscience deals with the science of materials and technologies in the scale range of 1-100 nm. This means nanoscience deals with a few hundred to a few thousand atoms or atomic clusters, whereas the microscopic word is made out of a trillion of atoms or molecules. Presently, nanoscience and technology represent the most active discipline all around the world and are considered as the fastest growing technology revolution in human history had ever seen. This intense interest in the science of the materials confined within the atomic scales stems from the fact that these nanomaterials exhibit fundamentally unique properties with the great potential of bringing a plethora of next-generation technologies in electronics, computing, optics, biotechnology, medical imaging, medicine, drug delivery, structural materials, aerospace, energy, etc [23]**.**

Nanotechnology is the application of science and technology to control matter at the molecular level, which is also referred to as the ability for designing, producing, characterization, and application to structures, devices, and systems by controlling shape and size at the nanometer scale. It emerges from the physical, chemical, biological, and engineering sciences where novel techniques are being developed to probe and manipulate single atoms and molecules. The technology springs from advancements in material science the ability to fabricate nanoscale materials in a uniform and reliable manner, at a reasonable scale and cost, and has turned many of our dreams true by enabling the construction of micro/Nano devices [24]**.**

Zinc oxide is attracting much attention because of its environmental stability and low cost as well as a high photo-catalytic ability but its application is limited only to the UV region; shorter than 385 nm as a result of its wide bandgap, in turn, limits the use of pure zinc oxide [25].

2.2. Aloe vera leaf and its medicinal properties

Plants are rich sources of various medicinally important substances and they explore the huge diversity in therapeutic and clinical aspects of society from ancient times. Medicinal plants are powerful drugs and are used all over the world for the treatment of several chronic diseases. Due to their wide biological and medicinal properties, high safety margins, and lesser costs, there is a

great demand for herbal medicines in both developed and developing countries as a source of primary health care. *Aloe vera* is a shrubby, perennial succulent plant of the Liliaceae family having turgid leaves joined at the stem in a rosette pattern. This plant is also characterized by stemless large, thick, fleshy leaves having a sharp apex, and a spiny margin. The phytochemicals present in this plant are used for the synthesis of nanoparticles. *Aloe Vera* possesses secondary metabolite primarily Alkaloids, Tannins Phenolic groups, and Flavonoids which support in the reduction of metal salt to metal oxide nanoparticles. The medicinal effect of *Aloe vera* includes antifungal activity, antidiabetic effects, anti-inflammatory, anticancer, and promotion of wound healing [26].

Figure 2 : Aloe vera plant

2.3. Synthesis of ZnO nanoparticles

Nanoparticles can be produced using many different techniques, typically classed as “top-down” (physical) and “bottom-up” (chemical and biological) methods. In top-down approach, nanoparticles are formed by size reduction method that means suitable bulk material reduces to small units. The bottom-up approach involves the generation of nanoparticles from small units like molecules and atoms or through the self-assembly of atoms into new nuclei, which further grow into a particle possessing nanoscopic dimensions [27]. The most commonly applied approach is bottom-up approach.

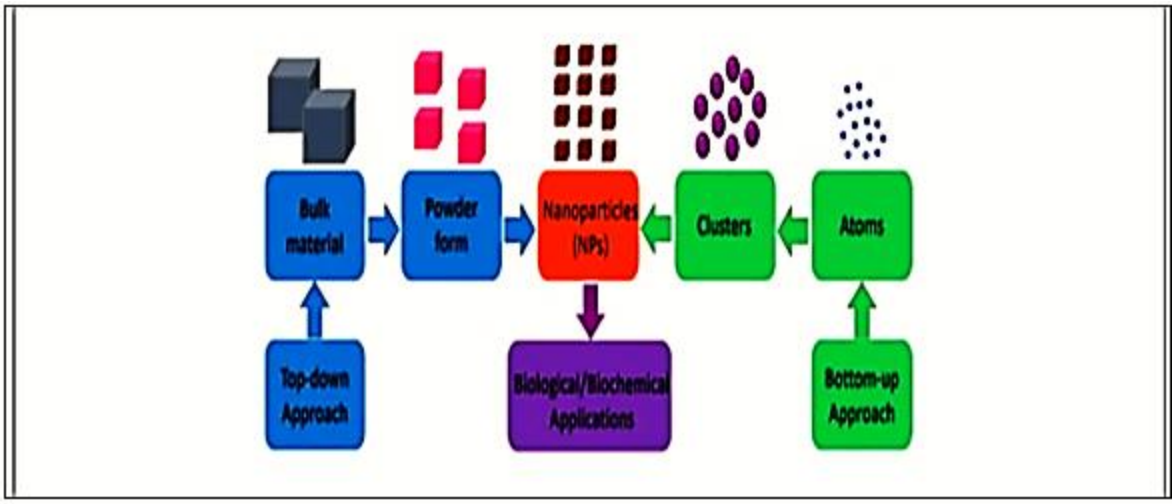

Figure 3 : Different methods used for the synthesis of NPs [28]

2.3.1. Physical methods

In this process, the physical forces are used as an attraction of nanoscale particles for the formation of stable and well-defined nanoparticles. Examples are amorphous crystallization, colloidal dispersion method, physical fragmentation, and vapor condensation. Among the physical methods of ZnO NPs synthesis, plasma method, laser ablation, and thermal evaporation are the most commonly used [29]. Previous studies have shown that laser ablation method offers some unique benefits because it allows the production of narrow distribution of size, shape, and well-purified ZnO NPs [30]. The efficiency and morphological identities of ZnO NPs synthesized using the laser ablation methods depend largely on the ablation time and wavelength of the laser [31]. Thermal evaporation is another form of physical method in which powdered source materials are vaporized at high temperature and the resultant vapor phase is condensed under high pressure to form desired ZnO NPs [32]. ZnO NPs synthesized using this approach has a potential photocatalytic activity which is recommendable for degradation. The physical methods suffer some limitations because they involve the usage of expensive equipment, large space for machine set up, and high pressure and temperature [33].

2.3.2. Chemical Methods

Micro-emulsion, chemical reduction, precipitation, hydrothermal techniques, and sol-gel are the most common chemical methods of synthesizing ZnO NPs [34]. Among these methods, sol-gel synthesis is the most commonly used method, which uses chemical reagents and zinc precursor

salt with the regulation of the solution pH to prevent precipitation of $Zn(OH)_2$. Thereafter, the solution is treated thermally under high temperatures to obtain ZnO NPs. Stabilizers like citrates or polyvinylpyrrolidone are usually added during synthesis to control the morphological properties and to prevent the agglomeration of ZnO NPs [35]. The concentration of zinc precursor and other reagents used during synthesis has been reported to significantly affect the shape and size of ZnO NPs produced. Variation in concentration of zinc precursor and reagent has been utilized in obtaining ZnO NPs with sizes in the range of nanometers to micrometers [35]. However, the chemical method suffers some limitations because they require high energy, toxic reagents, and expensive equipment. Findings have shown that traces of toxic reagent used during synthesis are detected in synthesized nanoparticles which could be hazardous and also limit its applications[36].

2.3.3. Biological Methods

The biological method of synthesizing ZnO Nps is referred to as green synthesis or biosynthesis. This method involves the use of microorganisms such as algae, fungi, yeast, bacterial, and plant extracts as the reducing agent [37]. Despite the advantages attached to the use of microorganisms as a reducing agents in the synthesis of ZnO NPs, the extreme safety required due to the toxicity of some microorganisms and challenges of incubation are the major problems [38].The biological methods which use plants is more preferable because of its nontoxicity, tranquil scaling-up, and reproducibility in making [39]. The high effectiveness of plant extracts in the synthesis of ZnO NPs has been attributed to the presence of high concentrations of chemical constituents termed phytochemicals or secondary metabolites they contain. Phytochemicals such as tannins, phenolic acids, terpenoids, flavonoids, alkaloids, and saponins have been reported as good reducing agents of zinc precursors [40]. This use of plant extract has some benefits such as being safe, cost-effective, environment friendly, nonhazardous, bio-compatible, and large-scale production is plausible [41].

Table 1: Comparison between the plant extract and another microorganisms system [42].

Biological source	Plant	Microorganism
Preparation time	Short	Longer than plant due to incubation time
Components responsible for reducing metal salts	Phytochemicals	Enzymes/proteins
Production yield	High	Lower
Solvent	Water	Natural source/extract
Cost	Effective	Less effective
Synthesis process	One-pot	More complicated
The location of nanoparticles formation	Intracellular, and extracellular	Intracellular synthesis and extracellular synthesis

2.4 Mechanism of Zinc Oxide Nanoparticles Formation

For nanoparticle synthesis mediated by plant leaf extract, the extract is mixed with metal precursor solutions at different reaction conditions. Plant constituents like; terpenoids, polyphenols, alkaloids, phenolic acids play an important role in the biosynthesis of zinc oxide nanoparticles. Flavonoids are Polyphenolic compounds and contain various functional groups that are capable of donating electron for the reduction of Zn^{2+} ions to ZnO NPs formation as shown on Figure 4. The active ingredient responsible for the reduction of Zn^{2+} ions varies depending upon the plant extract used or bioactive molecules [43].

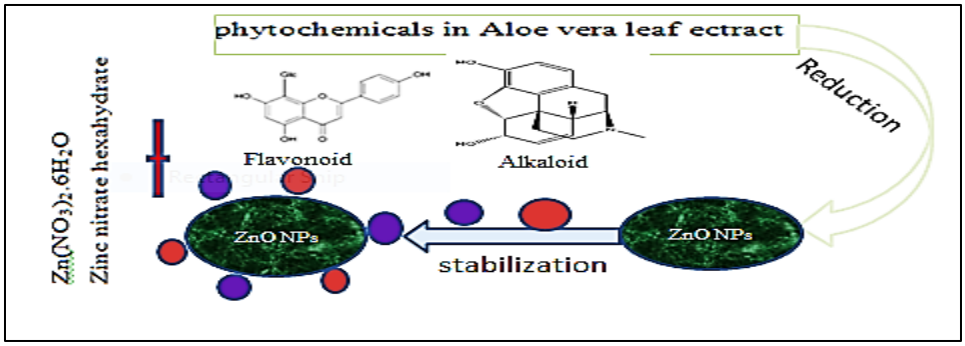

Figure 4: Schematic diagram for biosynthesis of ZnO NPs using plant

2.5. Metal doping

The introduction of metals such as silver, magnesium, and copper provides a synergistic effect with the semiconductor in a wide variety of applications such as wastewater treatment, optical and electronic devices. Babu and Antony [44] had investigated the effect of silver (Ag) doping on the ZnO nanoparticles synthesized using *Sida rhombi folia* leaves via a green approach. In terms of morphology, Ag doping increased the crystallite size of ZnO nanoparticles from 3.42 nm to 4.21 nm and caused a more agglomerated structure as compared to pristine ZnO nanoparticles. The research had also revealed that the presence of Ag dopants could promote the photocatalytic efficiencies of ZnO nanoparticles from 87% to 95% and from 55% to 95% in the degradation of malachite green and methylene blue respectively after 2 h of exposure to UV irradiation [45]. This was attributed to the role of Ag as an electron sink that improved the separation efficiency of electron-hole pairs and hence enhanced the generation of free radicals to mineralize the organic compounds. In addition, Khan et al. [46], had introduced the surface modification of ZnO nanoparticles using metallic copper (Cu) by the means of the green route. In the work, the presence of Cu as dopants had resulted in the decrement of bandgap energy from 3.378 eV to 3.30 eV. These properties were beneficial to the application of ZnO nanoparticles as photocatalysts in wastewater treatment due to the increment of active sites available for radical generation. Besides, the surface modification brought to the improvement in the biological activities of ZnO nanoparticles such as antibacterial, antifungal, and anticancer activities

Table 2: Doping of green synthesized ZnO nanoparticles

Dopant	Zn precursor	Green source	Particle size	Bandgap	Change in particle size	Change in band gap energy	Application	Reference
Cu	Zinc nitrate	Abutilon indicum leaves	-	–	Increased	-	Photocatalytic degradation, antibacterial	[46]
Ag	Zinc acetate	Pedalium murex L.leaves	108 nm	2.75 eV	Increased from 50.73 nm to 108 nm	Decreased from 3.37 to 2.75 eV	Photocatalytic degradation	[47]
Ni	Zinc nitrate	Brassica rapa leaves	-	-	Decreased	-	Antibacterial activity and seed germination	[48]
Mn	Zinc acetate	Ocimum tenuiflorum leaves	-	3.96 eV	Decreased	Decreased from 3.99 to 3.96 eV	Photocatalytic degradation	[49]
Fe	Zinc acetate	Hibiscus rosasinensis leaves	15–170 nm	3.34 eV	Decreased from 130 nm to 92.5 nm	Decreased from 3.39 to 3.34 eV	Photocatalytic degradation, antibacterial	[50]
Mg	Zinc nitrate	Pisidium guvajava leaves	78–100 nm	-	-	-	Optical devices	[51]
Au	Zinc acetate	Ziziphus jujube leaves	50–80 nm	-	-	-	Photocatalytic degradation	[52]
($ZnAl_2O_4$)	Zinc nitrate	Tragacanth gum	25–30 nm	3.05 eV	-	-	Photocatalytic degradation	[53]

2.6. Properties of zinc oxide nanoparticles

The semiconductors with the dimensions in the nanometer are important because of their electrical, optical and chemical properties which can be tuned by the changing the size of particles [54].

2.6.1. Electrical properties of Zinc oxide

The fundamental study of the electrical properties of ZnO nanostructures is crucial for developing their future applications in nano electronics. ZnO has a moderately large bandgap of 3.3 eV at room temperature. The benefits of a large bandgap comprise higher values of breakdown voltages, sustaining large electric fields, high-temperature and high-power operations. ZnO has n-type character, in the absence of doping. The origin of n-type character is typically the non-stoichiometry analysis. Due to the imperfections like the oxygen vacancies, and zinc interstitials, ZnO nanowires are reportedly show n-type semiconductor behavior. The major hindrance of ZnO is the broad series of applications in electronics and photonics with the complexity of p-type doping. The favorable and advantageous p-type doping for ZnO nanostructures will enormously enhance their upcoming advance applications in nano scale electronics and optoelectronics. The p-type and n-type ZnO nanowires can serve as p-n junction diodes and the light emitting diodes (LED) [39].

2.6.2. Optical properties of zinc oxide

ZnO is a wide band gap of 3.37 eV semiconductors with a large exciton binding energy of 60 meV and also considered as one of the most promising semiconductor material for electronic, photonic, optical and biological applications [40]. It is considered as the photoconductive under the analytical study of ultra violet light. The arrangement of optical and semiconductor properties construct a doped zinc oxide which is contend or for new generations of devices. Solar cells require intrinsic optical properties of ZnO nanostructures, which are being intensively deliberated for implementing photonic devices. Exciton emissions have been examined from the photoluminescence spectra of the ZnO nanorods. It is shown that quantum size confinement can significantly enhance the exciton binding energy. Strong emission peak at 380 nm due to band-to-band transition and green-yellow emission band related to oxygen vacancy are observed [55].

Photoluminescence spectra show that the ZnO nanowire is a capable and promising material for the UV emission. Its UV lasing property is additionally more significant and interesting. The additional advantages of ZnO nanowire lasers are that the exciton recombination lowers the threshold of lasing, and quantum confinement yields a substantial density of the band edges and enhances radioactive efficiency. Optical wave guiding using dielectric nanowire also achieved considerable progress.

In recent times, ZnO nanowires were stated as sub-wavelength optical waveguide. Optically forced light emission was guided by ZnO nanowire and coupled into SnO_2 Nano ribbon. These discoveries show that the ZnO nanostructures can be potential building blocks for integrated optoelectronic circuits. Optical properties have a great interest towards the vast application of optoelectronics, photovoltaic and biological sensing [41].

2.6.3. Chemical properties of zinc oxide

Zinc oxide occurs as the mineral zincite or as white powder known as zinc white. It is usually orange or red in color due to manganese impurity. Crystalline zinc oxide is thermo chromic in nature which changes from white to yellow color when heated and turns back to white color on cooling. This change in color is caused by a very small loss of oxygen at high temperatures. Zinc oxide is amphoteric in nature, which reacts with both acids and alkalis. When ZnO reacts with acid, it forms zinc sulfate. Similarly when it reacts with alkali, it forms zincates. ZnO decomposes to form zinc vapor and oxygen indicating its considerable stability. Exposure of zinc oxide to air absorbs both water vapor and carbon dioxide and forms zinc carbonate [42]

2.7. Antibacterial activity of ZnO nanoparticles

The biological method of the ZnO NPs synthesis is gaining importance due to its simplicity, eco-friendliness and extensive antimicrobial activity [43]. The main factor for the increase of the resistance pathogenic bacteria is over use of antibiotics and this has led to the emergence and spread of resistant pathogens and resistant genes in them [44]. The studies about toxicity have shown that zinc ions do not cause any damage to the DNA of human cells.

Nanoparticles as antimicrobial agents are their better efficiency on resistant bacteria, less toxicity and heat resistance. The possible mechanism for the bactericidal activity involves the factors including mainly reactive oxygen species (ROS) and the release of Zn ion (Figure 4). It has been found that the activity depends up on crystallite size, morphology, composition, specific surface

and phase of crystalline material [56]. Because of larger surface area than the bulk and distinguishable porosity as the particle size reduces, greater number of reactive oxygen species (ROS), namely O^{2-} hydrogen peroxide (H_2O_2), OH^-, and organic hydro peroxides are generated due to small crystallites, which in turn are considered responsible for the damage of cellular composition such as lipids, phosphorus-containing elements (DNA) and disabling of proteins by oxidative stress [57]. It should be noted that oxidative stress results when reactive oxygen species production surpasses the capability of antioxidant defense of the cell. Moreover, that the ZnO nanoparticles have positive zeta potential. Owing to this, nanoparticles provide enhanced particle surface reactivity and adherence with the microbial pathogens, and so surface properties also affect the interactions with the cell walls of the bacteria by allowing easy penetration into the bacteria. The exposure of nanoparticles to the surface of bacteria or accumulation of nanoparticles in the cell or even in the cytoplasm inhibit several functions in the cell thereby inducing structural abnormalities such as distraction of cellular function or deformation or rupture or blebs in membranes, leading eventually to death of bacterial cells.

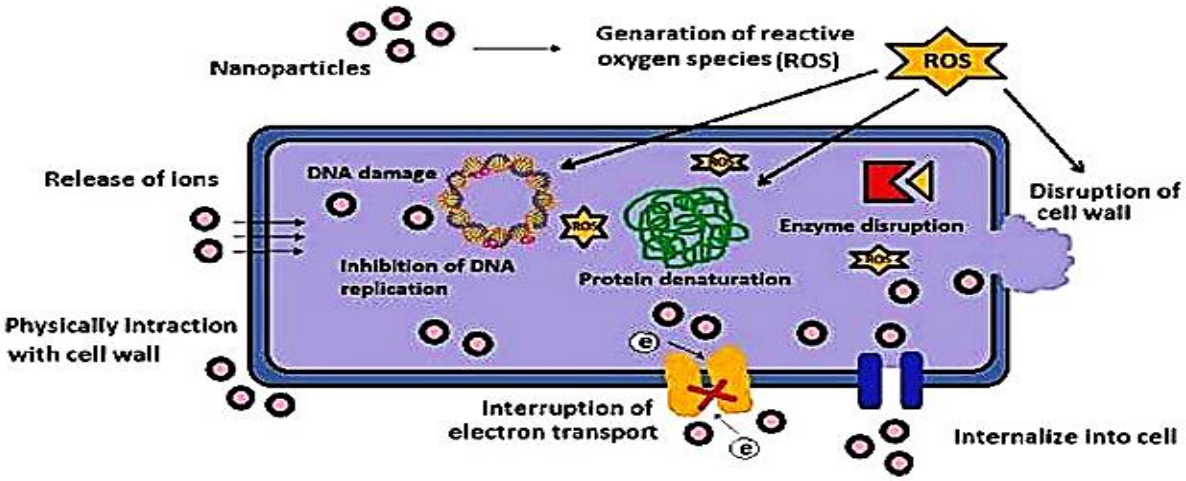

Figure 5: Various mechanisms of antimicrobial activity of the metal nanoparticles [58]

2.8. Photocatalytic degradation of dyes

Photocatalysts are invariably semiconductors activated by adsorbing a photon and can accelerate a reaction without being consumed. Photocatalysis process utilizes semiconductor photocatalysts to carry out a photo-induced oxidation process to break down organic contaminants [59]. Currently, semiconducting oxide photocatalysts are getting attention due to their efficiency in degrading recalcitrant organic compounds and can provide very good results either for complete

mineralization of dyes or for transformation into less complex and easily biodegradable structure. Semiconductor based heterogeneous photocatalysis called advanced oxidation process (AOP) is suitable for the oxidation of a wide range of organic compounds [60]. Among various photo catalysts, the semiconductor metal oxides, TiO_2 and ZnO are widely used in the degradation of organic pollutants because of their environmental feasibility, extreme photocatalytic activity, and production simplicity.

2.8.1. Advanced oxidation processes

Currently, advanced oxidation processes (AOPs) have been effectively and completely mineralizing recalcitrant dyes present in textile wastewater. These processes simply under the photon and thermal condition, the higher oxidation state of metal ion complexes generated hydroxyl radicals, which is the most powerful oxidizing agent after fluorine. Then, these hydroxyl radicals react with organic matter that leads to the destruction of toxic matters [60].

2.8.2. Mechanism of photocatalytic degradation

Photocatalytic reaction primarily depends on wavelength (light) (photon) (energy) and the catalyst. Generally, semiconducting materials are used as a catalyst as sensitizers due to their electronic structure for the irradiation of light stimulated redox process, which is characterized by a filled valence band and an empty conductions band.

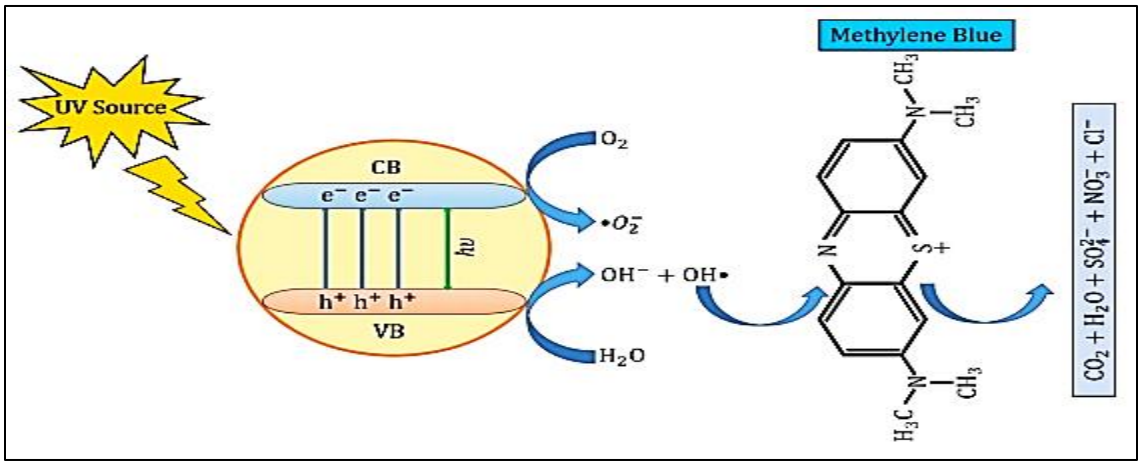

Figure 6: Degradation mechanism of MB dye by ZnO NPs under UV irradiation [61]

$$\text{Semiconductor} + \text{Light Energy} \longrightarrow \text{Semiconductor}\ (e^-_{CB} + h^+_{VB})$$

$$\text{Dye} + \text{Semiconductor}\ (h^+_{VB}) \longrightarrow \text{oxidation process}$$

$$\text{Semiconductor}\ (h^+_{VB}) + H_2O \longrightarrow \text{Semiconductor} + H^+ + OH^-$$

$$\text{Semiconductor}\ (h^+_{VB}) + OH^- \longrightarrow \text{Semiconductor} + OH^\bullet$$

$$\text{Dye} + \text{Semiconductor}\,(e^-_{CB}) \longrightarrow \text{reduction process}$$

$$\text{Semiconductor}\,(e^-_{CB}) + O_2 \longrightarrow \text{Semiconductor}\,(e^-_{CB}) + O_2^{\bullet-}$$

$$O_2^{\bullet-} + H^+ \longrightarrow HO_2$$

$$HO_2 + HO_2 \longrightarrow H_2O_2 + O_2$$

$$H_2O_2 + O_2^{\bullet-} \longrightarrow OH^{\bullet} + OH^- + O_2$$

$$\text{Dye} + OH^{\bullet} \longrightarrow \text{Degradation product [60]}$$

When light energy or photons fall on the surface of a semiconductor photocatalysts process, it gives three fundamental changes. If the amount of energy to the incident ray equal or greater than the bandgap energy of the semiconductor, the valence band electrons become restless and forced to move to the conduction band of the semiconductor. Secondly, holes are left in the valence band of the semiconductor. These holes in the valence band can oxidize donor molecules and react with water molecules to generate hydroxyl radicals (The hydroxyl radicals have strong oxidizing power responsible for the degradation of pollutants). Thirdly, electrons in the conduction band react with dissolved oxygen species to form superoxide ions. These electrons induce the redox reactions. These holes and electrons could undergo successive oxidation and reduction reactions with any species, which might be adsorbed on the surface of the semiconductor to give the necessary products [60].

2.8.3. Factors affecting the photo degradation

Efficiency of the photocatalytic system is highly dependent on different operational parameters such as, concentration of dye, amount of photocatalyst, pH of the solution and time of irradiation.

Effect of initial concentration of dye in the solution: Because photocatalysis is mainly dependent on the passage of light through the solution, the degradation will decrease with an increase in dye concentration. It will also affect the irradiation time required for the degradation to attain complete mineralization. Previous reports have shown that the rate of degradation is inversely proportional to the initial concentration of the pollutant

Effect of amount of catalyst: As the amount of catalyst increases there will be an increase in the number of active sites, thus an increase in the production of the hydroxyls and superoxide species responsible for degrading the pollutant. With an increase in the amount of catalyst there is an increase in the degradation rate, which is a feature of heterogeneous photocatalysis. There

is an increase up to an optimum point where the amount of catalyst will disturb the passage of light into the solution [62].

Effect of pH: The pH of the solutions affects the electrostatic interactions between the contaminants and the charged particles. Therefore the pH of solution is important as it interferes with the surface charge properties of the photocatalyst; it therefore shifts the potentials catalytic reactions. For most photocatalysts excess H^+ and OH^- have been found to decrease the reaction rate [60].

3. MATERIALS AND METHODS

3.1. The study area and period

The study was carried out from March to September 2021; at the Chemistry laboratory, Jimma University main campus, which is 346 Km southwest of Addis Ababa, Ethiopia.

3.2. Materials

3.2.1. Chemicals

Zinc (II) Nitrate hexahydrate (Zn $(NO_3)_2.6H_2O$), Copper (II) Nitrate trihydrate (Cu $(NO_3)_2.3H_2O$), Sodium hydroxide (NaOH), Gentamycin, dimethylsulfixode (DMSO), Muller-Hinton agar, Ethanol absolute (99.9%), Methylene blue and deionized water. All chemicals were analytical grade and used without further purification.

3.2.2. Apparatus and instruments

The laboratory apparatus used for this work include drying oven, Mortar with Pestle, Digital balance, Magnetic stirrer with hot plate, crucible, Watch, Centrifuge, Cuvettes, Whatman filter paper No 1, Beakers(50 mL,100 mL and 250 mL), Test tubes, Droppers, Graduated measuring cylinders, Glass rod and instruments; Ultraviolet–Visible Spectroscopy (PerkinElmer spectrum Lambda 25), Fourier transform infrared spectrometry (PerkinElmer spectrum Two), X-ray diffraction (Drawell XRD 7000) and Scanning electron microscopy (SEM JCM-6000Plus).

3.3. Method

3.3.1. Sample collection and Preparation

Fresh *Aloe vera* plant was collected from Limmu Seka woreda around the local area of Dora Gibe. The selected part of the plant shoot was cut, washed twice with tap water followed by distilled water to remove dust particles and other contaminants. Then, it was dried at room temperature. The dried *Aloe vera* samples were ground as a fine powder using mortar and pestle. Then, 5 g of powder was boiled in a 250 mL beaker containing 100 mL of deionized water for 30 min at 60 ^{o}C [63], and the color changed from watery to light brown was formed. The solution was cooled and filtered with Whatman filter paper No 1 to get the *A. Vera* leaf extracts. Finally the obtained extract was stored at room temperature in order to be used for synthesizing the nanoparticles (Appendix 1).

3.3.2. Phytochemical screening test

A phytochemical screening test was conducted to confirm the presence of various components in the leaf extract.

Flavonoids: Formation of yellow colour when 2 mL of the extract was treated with 2 mL of NaOH solution indicated the presence of flavonoids.

Tannin: 2 mL of extract was mixed with 2 mL of distilled water and few drops of $FeCl_3$ solution (5% w/v) were added. Formation of a green precipitate indicates the presence of tannins [64].

Saponins: 1 mL of solvent extract was introduced into a tube containing 1 mL of distilled water and agitated in a measuring cylinder for 15 min. The formation of 1 cm layer of foam shows the presence of saponins in the extracts [64].

Alkaloids: 3 mL of aqueous plant extract was stirred with 1% hydrochloric acid (HCl), and filter using filter paper. To the filtrate Wagner reagent was added. Reddish-brown precipitate was formed which show the presence of alkaloids [26].

Phenolic: 2 mL of the leaf extract was treated with 4 drops of ferric chloride ($FeCl_3$) solution. A change in the solution to bluish black precipitates confirmed the presence of phenolic compounds [65].

3.3.3. Optimization of synthesis parameters for zinc oxide nanoparticles

Concentration of precursor salt solution: The effect of precursor salt concentration was optimized for the optimum synthesis of the metallic nanoparticles by increasing the concentration of Zn $(NO_3)_2 \cdot 6H_2O$) solutions from 0.05 M to 0.125 M with keeping the volume of the plant extract and pH constant. The absorbance (200 to 800 nm) of the resulting nanoparticles solution was measured by UV-Vis Spectroscopy.

Plant extract: The volume of the plant extract was optimized by increasing the concentration of plant extract (10, 20, 30, 40, and 50 mL) in 100 mL of precursor salt solution. The absorbance (200 to 800 nm) of the resulting nanoparticles solution was measured by UV-Vis Spectroscopy.

Solution of pH: The pH of the reaction was optimized by increasing the pH from 8 to 13. The pH was adjusted using 0.1 M HCl and 0.1 M NaOH. After pH adjustment, absorbance (200 to 800 nm) of the resulting nanoparticles solution was measured by UV-Vis Spectroscopy

3.3.4. Synthesis of ZnO nanoparticles

Zinc oxide nanoparticles were successfully synthesized by green synthesis method using Zinc nitrate hexahydrate ($Zn(NO_3)_2 \cdot 6H_2O$) [66]. 0.1 M Zinc (II) nitrate solution was prepared by dissolving 2.795 g of Zinc nitrate hexahydrate in 100 mL deionized water using a 250 mL beaker. 10 mL of *Aloe vera* leaf extract was added and stirred for 5 min. To adjust pH to pH-8, 10 mL of 2 M NaOH was added to the solution while stirring. Next, the mixture was stirred continuously at 60 °C for 2 h and the white-colored precipitate was observed in the solution**.** The precipitate was collected and centrifuged for 5 min. Then, the precipitate was washed with distilled water three times followed by ethanol to remove the impurity of all the ions produced during the reaction. Finally, the precipitate was collected to the crucible, dried in an oven at 60 ^oC for 2 h, and ground to a fine powder using an agate mortar and pestle for further characterization and to evaluate its activities (Appendix 2).

3.3.5. Synthesis of Cu-doped ZnO nanoparticles

Both 1% Cu-doped ZnO and 4% Cu-doped ZnO nanoparticles were synthesized using the same procedure of the synthesized ZnO NPs [67]. 0.028 g and 0.1 g of Cu $(NO_3)_2.3H_2O$ were added to 0.1 M of 100 mL Zn $(NO_3)_2.6H_2O$ to obtain 1% Cu-doped ZnO (0.001 M), and 4% Cu-doped ZnO NPs (0.004 M) respectively. For both synthesized, the mixtures were stirred continuously using a magnetic stirrer for 5 min. 10 mL *Aloe vera* leaf extract was added and was stirred for 10 min to make homogeneity. To adjust pH to pH 8, 15 mL 2 M of NaOH was added while stirring. After the addition of NaOH, the solution was stirred for 2 h at 60 ^oC and the yellowish blue color solution was obtained. Then, the precipitate was collected, centrifuged for 5 min, and washed with distilled water three times followed by ethanol. Finally, the precipitate was dried in an oven at 60 ^oC for 2 h and ground to a fine powder using an agate mortar and pestle for further characterization and to evaluate its activities (Appendix 3).

3.4. Characterization of ZnO and Cu-doped ZnO Nanoparticles

3.4.1. UV-Visible Spectroscopy

The optical characterization of synthesized ZnO and Cu-doped ZnO NPs was carried out using UV-Vis Spectroscopy in the wavelength region of 200 nm - 800 nm.

3.4.2. Fourier Transform Infrared (FT-IR) Spectroscopy

The plant extract, synthesized ZnO and Cu-doped ZnO nanoparticles were characterized by Fourier Transform Infrared. FT-IR analyzes and detects surface functional groups at the scanning range of 4000 – 400 cm^{-1}. By FT-IR characterization, the sample was mixed with solid KBr uniformly and properly, which was compressed to settle down on a thin transparent film and this thin transparent film was for FT-IR analysis which was kept in the chamber of the instrument for scanning.

3.4.3. X-Ray Diffraction (XRD)

The crystalline structure of the green synthesized ZnO and Cu-doped ZnO nanoparticles were characterized by X-ray diffraction using X-ray diffractometer. XRD spectrum was recorded from 20^o to 80^o with 2θ angles using Cu-Kα (λ =1.54 Å) radiation operated at 30 kV and 25 mA. Debye Scherrer's Eq. (1), was used to calculate the crystallite size.

$$D = \frac{k\lambda}{\beta \cos\theta} \qquad (1)$$

Where D is the Crystallite size, k=0.9, λ-is the X-ray source wavelength, β is the Full Width at Half Maximum (FWHM) of a peak, and θ = is the Bragg diffraction angle.

3.4.4. Scanning electron microscopy (SEM)

In this research work, JCM-6000Plus SEM machine was employed to study the morphology of synthesized nanoparticles. The experiment was performed at an accelerating voltage of 30 kV. The slide was coated with platinum and after the platinum coating, the SEM image was taken. SEM reveals information about the surface morphology of materials making up the sample. It also provides detailed high-resolution images of the sample by restoring a focused electron beam across the surface and detecting secondary or backscattered electron signal. In SEM characterization, nanoparticles powder is mounted on a sample holder followed by coating with a conductive metal. The sample is then scanned with a focused fine beam of electrons. The surface characteristics of the sample were obtained from the secondary electrons emitted from the sample surface.

3.5. Method for Antibacterial Activity

3.5.1. Preparation of Inoculum

Nutrient broth (1.3 g in 100 mL distilled water) was prepared in 4 conical flasks and sterilized. In the first two conical flasks clinically isolated strain of gram-positive bacteria: *Bacillus cereus*

and *Staphylococcus aureus* were inoculated. In the second two conical flasks clinically isolated strains of gram-negative bacteria, *Escherichia coli* and *S.typhi* were inoculated. These bacterial cultures inoculated in nutrient broth were kept on a rotary shaker for 24 hours at 100 rpm [68].

3.5.2. Disc diffusion methods

Antibacterial tests were carried out by the disc diffusion method using the suspension of bacteria spread on nutrient agar. Antibacterial activity of plant extract, ZnO, 1 % Cu- doped ZnO and 4% Cu- doped ZnO nanoparticles were tested against gram-positive (*Staphylococcus aureus* and *Bacillus subtillis*) and gram-negative (*Escherichia coli* and *salmonella typhi*) bacteria by disc diffusion method. Bacterial cultures were maintained on nutrient Muller-Hinton agar at 37 ^{o}C and the cultures were kept inappropriate media slants and stored at 4^{o}c until used. The antibacterial activities were tested by the disc diffusion agar method, which is a test of the antibiotic sensitivity of the bacteria and it uses the antibiotic discs to test the extent to which bacteria are affected by those antibiotics. Discs were applied to the surface of an agar plate that was previously dried. The plates were, then turned upside down and incubated at 37^{o}c for 24 h in an incubator. The plates were shaken gently to allow the evenly mixing of bacteria cells and agar. Agar plate was divided into 6 sections plant extract, ZnO, 1% Cu- doped ZnO, 4% Cu-doped ZnO NPs sample, and for both positive(Gentamicin) and negative(DMSO) control. Then 100 mg of each sample was dissolved in 1 mL of DMSO, to obtain 100 mg/mL. From the sample, 100 µL of concentration saturated with discs (6 mm diameter disc) was placed on a plate and incubated at 37^{o}c for 24 h [57]. Clear inhibition zones formed around the discs indicate the presence of antibacterial activity [69]. The results were taken by considering the zone of growth, and antibacterial activity was evaluated by measuring the diameter (mm) of the inhibition zone (IZ) around the disc against the test organisms by using a ruler.

3.6. Evaluation of photocatalytic dye degradation

The photocatalytic activities of the synthesized ZnO and Cu-doped ZnO NPs were evaluated by the degradation of methylene blue (MB) under UV lamp irradiation (200 W) (Figure 7). 10 mg of methylene blue dye was added to 1000 mL of distilled water which was used as stock solution. About 50 mg of the synthesized ZnO and Cu-doped NPs were added separately to 100 mL of methylene blue dye solution. The suspension was magnetically stirred in the dark for 30 min to reach the adsorption-desorption equilibrium. Before exposure to visible light irradiation, 5

mL reaction mixture was centrifuged and absorbance of the supernatant was measured at a wavelength of 665 nm. Then, the mixture was placed under UV irradiation with stirring. The progress of the reaction subsequently followed at different time intervals using a UV-visible spectrometer. 5 mL reaction mixture was taken at a regular time interval of (30, 60, 90, 120, 150,180 min) and the solution was centrifuged for measurement [62].

The absorbance of the supernatants was measured periodically using a UV–visible spectrophotometer. As a control treatment, photolysis was conducted by directly exposing the UV source to MB solution without photocatalyst contains. The percentage of dye degradation (PD) was calculated using the following Eq. (2)

$$PD = \frac{(A_o - A_t)}{A_o} x100\% \quad \text{..... (2)}$$

Where A_o is the initial dye absorbance and A_t is the dye absorbance at time t.

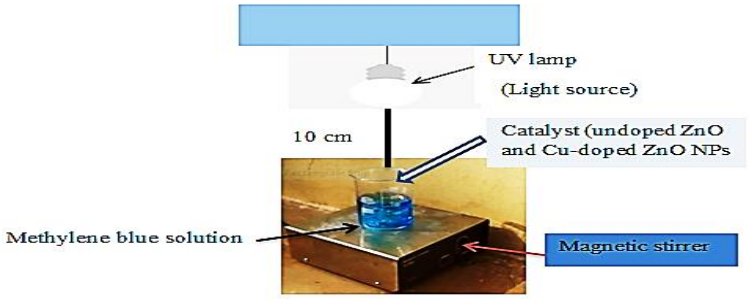

Figure 7: Experimental setup of photocatalytic degradation.

3.6.1. Determination of point of zero charge

Point of zero charges (PZC) is a fundamental description of the oxide surface. The batch equilibrium technique (solid addition method) was employed to determine the pH at PZC of the prepared samples as in the following procedure. Several samples of 0.1 g of Cu-ZnO were introduced into 20 mL of 0.1 M NaCl solution at different initial pHs (3, 5, 7, 8, 9, 10, 11, and 12). Initial pHs (pHi) of all suspensions were adjusted by using 0.1 M NaOH and/or 0.1 M HCl solutions. Then the suspensions of known pHi were stirred at room temperature, and allowed to equilibrate for 24 h. Next, the final pH values (pHf) were measured after a period of 24 h. The difference between both the initial and final pHs (ΔpH = pHf- pHi) was calculated and the graph was plotted between ΔpH and pHi [70]. In the plot, the point of intersection of the resulting curve at which ΔpH = zero is the pH PZC value of Cu-ZnO Nanoparticles (Appendix 4).

3.7. Methods of Data Analysis

Origin8.0, Jade 6.5, X-pert high score plus Philips XRD and match software were used to analyze the data collected from UV-Visible, XRD, FT-IR spectroscopy and point of zero charges data as well as Mendeley for citing the reference.

4. RESULTS AND DISCUSSION

4.1. Phytochemical screening analysis

The phytochemical screening test was carried out by using the aqueous leaf extract of *Aloe vera*. The plant extract is used as a potential substitute for stabilizing and reducing agents due to the combination of its bio-components such as Alkaloids, Tannins Phenolic groups, and Flavonoids (Table 3). Many reports have specified that phenols and flavonoids are involved in the bio-reduction, formation, and stabilization of metal and metal oxide NPs [26]. The presence of a large number of OH groups in phenol and flavonoids is responsible for reducing zinc nitrate into ZnO NPs. In the present study, phenols and flavonoids in the aqueous leaf extract bind the surface of zinc in zinc nitrate to activate the formation of ZnO and Cu-doped ZnO NPs and also control the size. The –OH groups from the phenol and flavonoid compounds responsible for the action of the reducing, capping and stabilizing agents [71].

Table 3 : Lists of Phytochemical screening of the *Aloe vera* leaf extracts

No	Phytochemicals	Color observed	Test performed.	Inferences
1	Alkaloids	Reddish-brown precipitate	Wagner`s test	+
2	Tannins	Yellow brown precipitates	ferric chloride	+
3	Saponins	Foam	Foam test	+
4	Flavonoids	Yellow color	alkaline reagent	+
5	Phenolic	White precipitate	ferric chloride	+

"+" show the presence of phytochemicals in *Aloe vera* leaf.

Moreover, the FTIR results (Figure 10) also supported the presence of functional group in aqueous leaf extract of *Aloe vera.*

4.2. Synthesis of ZnO and Cu- doped ZnO Nanoparticles by *Aloe Vera* Leaf Extract

Green synthesis method was used to fabricate the ZnO, 1%, and 4 % Cu-doped ZnO using the aqueous leaf extract of *Aloe vera*. Bio-reduction involves reducing metal ions to zero valence metal NPs with the help of phytochemicals. When colorless zinc nitrate was added with *Aloe vera*, a white colored precipitate was produced which show formation of ZnO NPs and when Colorless Zinc nitrate, blue Copper nitrate and light brown color of *Aloe vera* extract added to together yellowish blue color formed for both Cu-doped ZnO NPs.

4.2.1. Effect of precursor salt solution concentration

The results of this study on the effect of precursor salt solution showed that 0.1 M Zinc nitrate resulted in maximum nanoparticle formation with the absorbance peak at 358 nm. The absorption spectra intensity of nanoparticles increased with increased concentration of precursor salt solutions from 0.05 M to 0.1M accompanied by a sharpening of a peak. However, a further increase in concentration to 0.125 M resulted in a decrease in absorbance (Appendix 5). This is due to that higher concentration of zinc nitrate acts in favor of agglomeration of the zinc oxide particles rather than in the formation of capped zinc oxide nanoparticles in a colloidal solution [72].

4.2.2. Effect of volume of plant extract

The reducing agent in the formation of nanoparticles varies from plant to plant and the amount of the volume extracted in the reaction medium. The result indicated that when volume of extracted plant increase from 10 mL to 50 mL, the absorption peaks decrease and maximum absorption was observed with 10 mL of *Aloe vera* leaf extract in 100 mL of zinc nitrate (Appendix 6). That means, number of bioactive compounds present in the case of 10 mL was sufficient to reduce all Zn^{2+} ions present in the reaction mixture [73]. This indicated that low quantities of the extract can reduce zinc ions, but do not protect most of the quasi-spherical nanoparticles from aggregating because of the deficiency of biomolecules to act as Capping agents [74].

4.2.3. Effect of solution pH

The reaction solution of pH is considered an important parameter in nanoparticle synthesis. In this study, the solution was adjusted to different pH (8-13) with a concentration of 0.1 M zinc nitrate and 10 mL of plant extract. Maximum absorbance peak ZnO nanoparticles were found at pH 8 while, an almost straight absorption line with no peak was observed at pH 13, spectrum at pH 8 and 10 showed characteristic absorption peak. However, better absorbance and sharpness were recorded at pH 8 (Appendix 7). At high initial pH values (pH > 8), a higher amount of OH^- ions could function as strong complexing agents with Zinc(II) ions, thus interfering with the capping ability of biomolecules in plant extracts as well as competing with zinc (II) nitrate precursors for binding to the biomolecules [75].

4.3. Characterization and analysis of zinc oxide and Cu-doped zinc oxide nanoparticles

4.3.1. Ultraviolet-Visible spectra analysis:-

Synthesized samples were characterized by UV-Vis at Jimma University main campus. The absorption band at 358 nm, 365 nm, and 379 nm were observed for ZnO, 1% and 4% Cu-ZnO NPs respectively (Figure 8 and 9). These absorption peaks confirm the occurrence of the blue-shifted absorption spectrum concerning the bulk value (385 nm) [48]**.** The observed sharp bands indicated as the zinc ion is efficiently reduced by the *Aloe vera* leaf. The blue shift might be attributed to the smaller size of the nanoparticles. Moreover, it might be due to the quantum confinement effect which is in good agreement with the previous report [9]. The bandgap energies of these synthesized nanoparticles were obtained by plotting absorptivity $(\alpha hv)^2$ as a function of energy (hv). Extrapolating the linear portion of the curve to the absorption axis gave bandgap energies of 3.17 eV, 2.95 eV, and 2.83 eV for ZnO, 1% Cu-doped ZnO and 4% Cu-doped ZnO NPs, respectively. There was a decrease in bandgap energies from ZnO and Cu-doped NPs. The reason behind this decrease in bandgap energy from 3.17 eV to 2.95 eV and 2.83 eV [77], is due to Cu doping. 4% Cu-doped ZnO NPs exhibited less band gap energy value than 1% Cu-doped ZnO NPs because of the higher degree Cu doping [78].

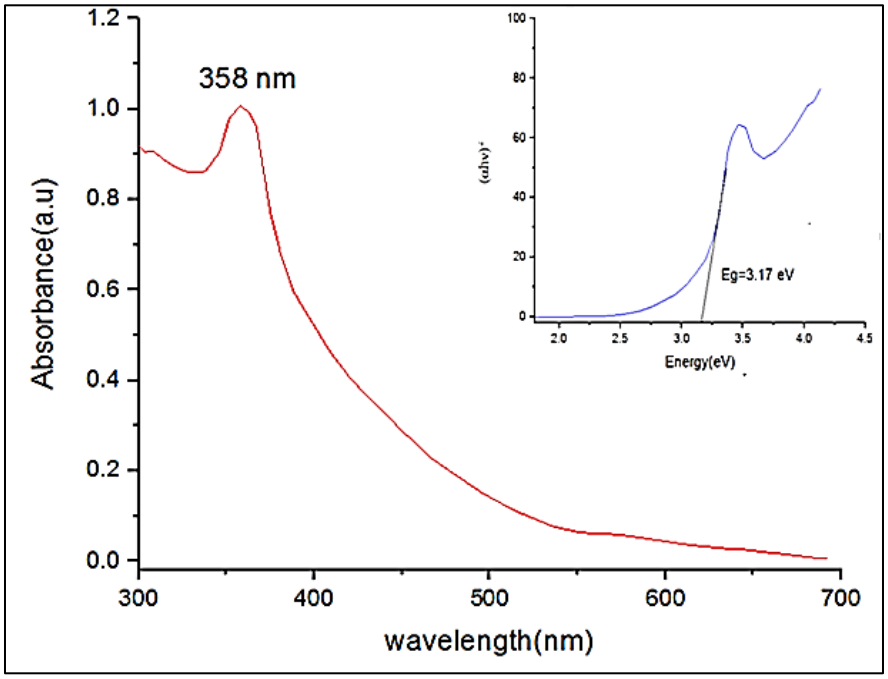

Figure 8: UV-Vis absorbance of ZnO NPs synthesized using Zinc nitrate hexahydrate and *Aloe vera* leaf extract

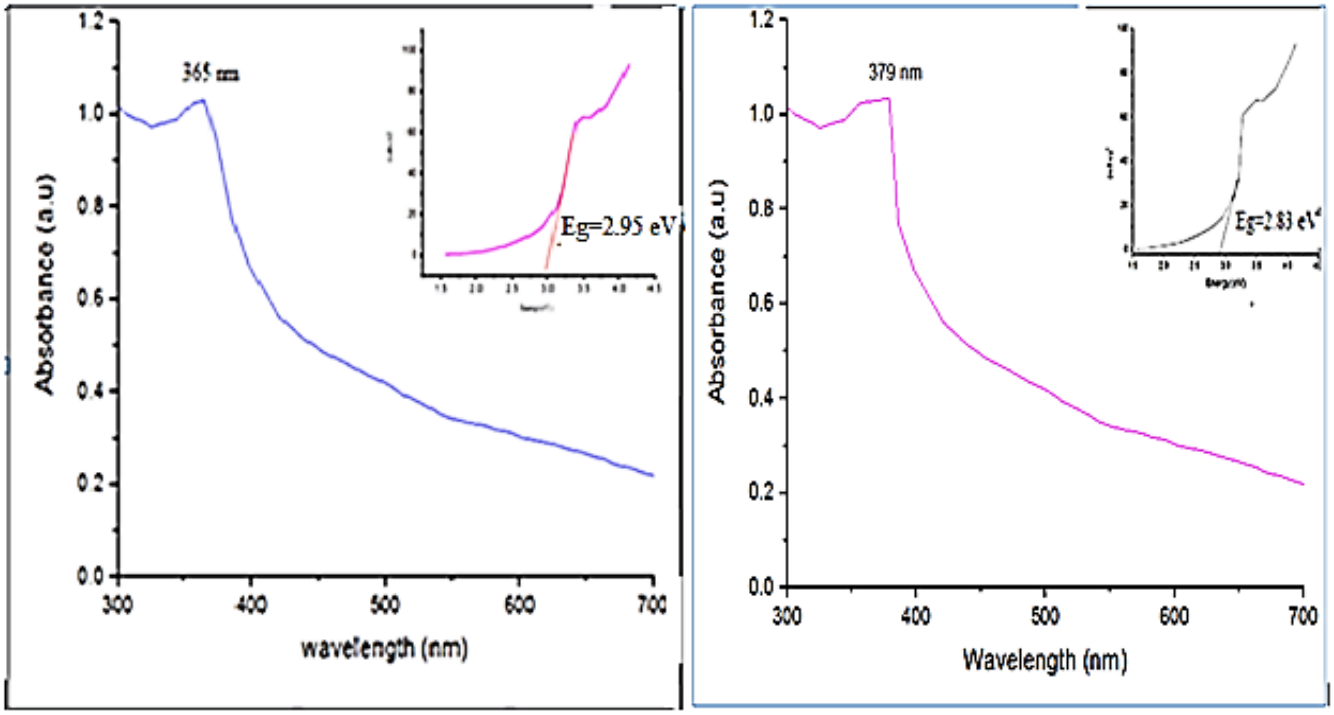

Figure 9 : UV-Vis absorbance of (a) 1% Cu-ZnO NPs (b) 4% Cu-ZnO NPs synthesized using Zinc nitrate hexahydrate and *Aloe vera* leaf extract**.**

4.3.2. Fourier Transformed Infrared (FT-IR) Spectroscopy Analysis

Synthesized samples were characterized at Addis Ababa University by FT-IR spectroscopy analyzer which was used for identification of different functional groups in the samples. It was analyzed at spectrum range of 4000–400 cm^{-1} wave number in percent transmittance using KBr pellet at room temperature**.** Figure 10 shows FTIR of *Aloe vera* leaf extract, ZnO, 1% Cu-ZnO, and 4% Cu- ZnO NPs. The broad peak in the higher energy region centered between 3404 and 3352 cm^{-1} is accredited to the hydroxyl group (OH) stretching vibrations which represents the presence of water molecules on the surface of synthesized nanoparticles. The small peak between 2933 and 2909 cm^{-1} is due to the C-H stretching vibration of alkane groups [79]. The peaks between 1606, and 1571 cm^{-1} due to the C=C stretch in the aromatic ring and C=O stretch in polyphenols. The characterized peaks observed at 1397 and 1384 cm^{-1} were due to C–C in-ring stretching of aromatics and C-N stretching vibration in the amine group [80]. Weak bands at 880 and 808 cm^{-1} are assigned to the vibrational frequencies due to the change in the microstructural

features by the addition of Cu into Zn–O lattice. As it can be seen in Figure 10, the intense absorption peak at 615-541 cm^{-1} is related to the stretching vibrations of Zn–O bond. FTIR spectrum wavenumber indicates the participation of polyols, and having functional group alcohols, phenols, alkanes, and aromatic in bio reduction reactions.

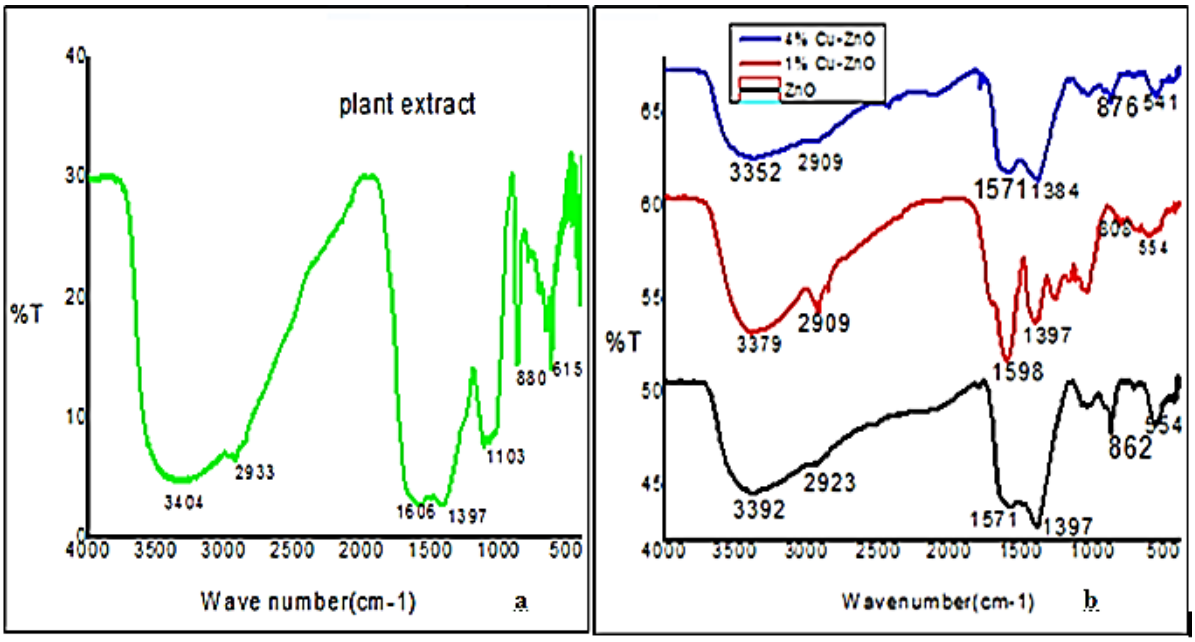

Figure 10: FTIR spectra of (a) plant extract, (b) synthesized ZnO NPs, 1% Cu- doped ZnO and 4% Cu- ZnO NPs.

As seen from Figure 10, synthesized ZnO, 1% Cu-doped ZnO and 4% Cu-doped ZnO NPs showed a small shift with slight changes to lower wavenumber (red shift) for the functional group of O-H bond, C-H stretching, primary amine and metal oxygen bond suggesting that biomolecules from the extract were capped or bonded to the surface of NPs.

4.3.3. X-ray diffraction (XRD)

X-ray diffraction (XRD) analysis was done at Jimma University Institute of Technology campus to determine crystallite size of the NPs. The XRD patterns for the three samples analyzed, i.e., ZnO, 1% Cu-doped ZnO, and 4 % Cu-doped ZnO NPs, are shown on Figures 11. The diffraction peaks are matched with the hexagonal wurtzite structure by comparison with the data from JCPDS No. 01-079-2205 which its 2θ= 31.76, 34.41, 36.25, 47.53, 56.59, 62.85, 67.94, 69.08, and correspond to the lattice planes (100), (002), (101), (102), (110), (103), (112), and (201) [81]. Furthermore, XRD analysis data showed well-resolved patterns of ZnO with no impurity

peaks present. The absence of characteristic peaks related to metallic Cu or its oxides separate phases suggests that the Cu ions have successfully incorporated into ZnO without affecting its crystal structure. This is due to the fact that ionic radius of Cu^{2+} (0.73 Å) is very close to that of Zn^{2+} (0.74 Å), due to which Cu can easily penetrate into ZnO crystal lattice [82].

The average crystallite size of each samples were calculated using the Debye– Scherrer formula, and the largest is 4% Cu-doped ZnO (24.91 nm), followed by 1% Cu-doped ZnO (23.74 nm) and ZnO (19.24 nm). The obtained results showed that the crystallite size of the NPs increased from 19.24 to 24.91 nm as Cu content was increased from 0% to 4%. The intensity of the diffraction increases with increment in Cu concentration, which also confirms the presence of Cu in the ZnO structure [78]. Similar result was reported for ZnO nanoparticles which its average crystallite size was 18-19 nm [63]. As shown in Table 4, small change in diffraction peaks of Cu-doped ZnO from ZnO is due to the increase of micro-strain [83].

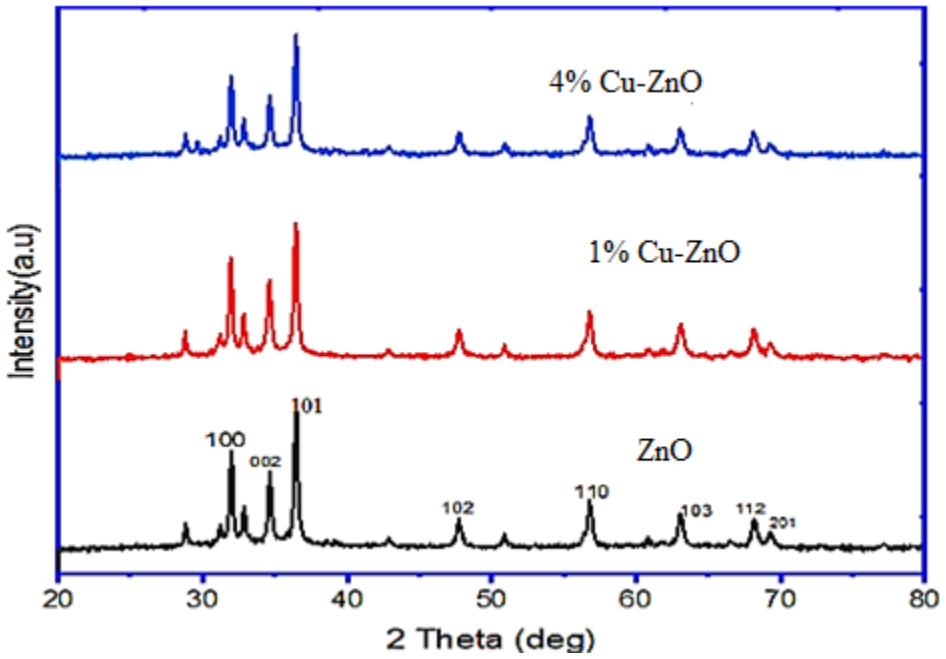

Figure 11: XRD spectrum of ZnO, 1% Cu-doped ZnO and 4% Cu- doped ZnO NPs

Table 4: XRD peak positions of ZnO and Cu-doped ZnO samples compared to standard values

(hkl) plane	For ZnO NPs			For 1% Cu-doped ZnO NPs			For 4% Cu-doped ZnO NPs		
	2θ (°)	FWHM (β)	Crystalline Size	2θ (°)	FWHM (β)	Crystalline Size	2θ (°)	FWHM (β)	Crystalline Size
100	31.83	0.3	25.47	31.76	0.3	25.47	31.75	0.3	25.47
002	34.5	0.36	21.07	34.43	0.3	25.29	34.43	0.3	25.29
101	36.321	0.3	25.16	36.24	0.36	20.97	36.23	0.36	20.97
102	47.631	0.36	20.19	47.52	0.36	20.2	47.52	0.36	20.20
110	56.685	0.42	16.65	56.60	0.36	19.43	56.58	0.36	19.43
103	62.973	0.48	14.11	62.87	0.48	14.12	62.81	0.36	18.83
112	68.06	0.42	15.68	67.94	0.42	18.30	67.93	0.42	15.69
201	69.4	0.42	15.551	69.16	0.48	20.10	69.16	0.42	22.97
Average crystal size			19.24 nm			23.74 nm			24.91 nm

4.3.4. Scanning Electron Microscopy (SEM) Analysis

Synthesized samples were characterized at Adama Science and Technology University by scanning electron microscopy to determine crystal morphology. The SEM images of ZnO and Cu-doped ZnO NPs are shown on Figure 12 (a – c). The results reveal that the surface morphology of ZnO NPs altered with increasing in Cu concentration. SEM morphology of synthesized ZnO nanoparticles shows a mixture of spherical and irregular NPs. The nanoparticles were also agglomerated and varied with doping content of copper as depicted on Figure.12 (b, and c). This result is consistent with the result obtained by Khan et al [48]. SEM image showed crushed-ice, spherical shapes and agglomerated Cu-doped ZnO NPs. However, the ZnO showed lower agglomeration compared to 1% Cu-doped ZnO and 4% Cu-doped ZnO NPs. This suggests that Cu aided the development of secondary particles through agglomeration of elementary particles [81].

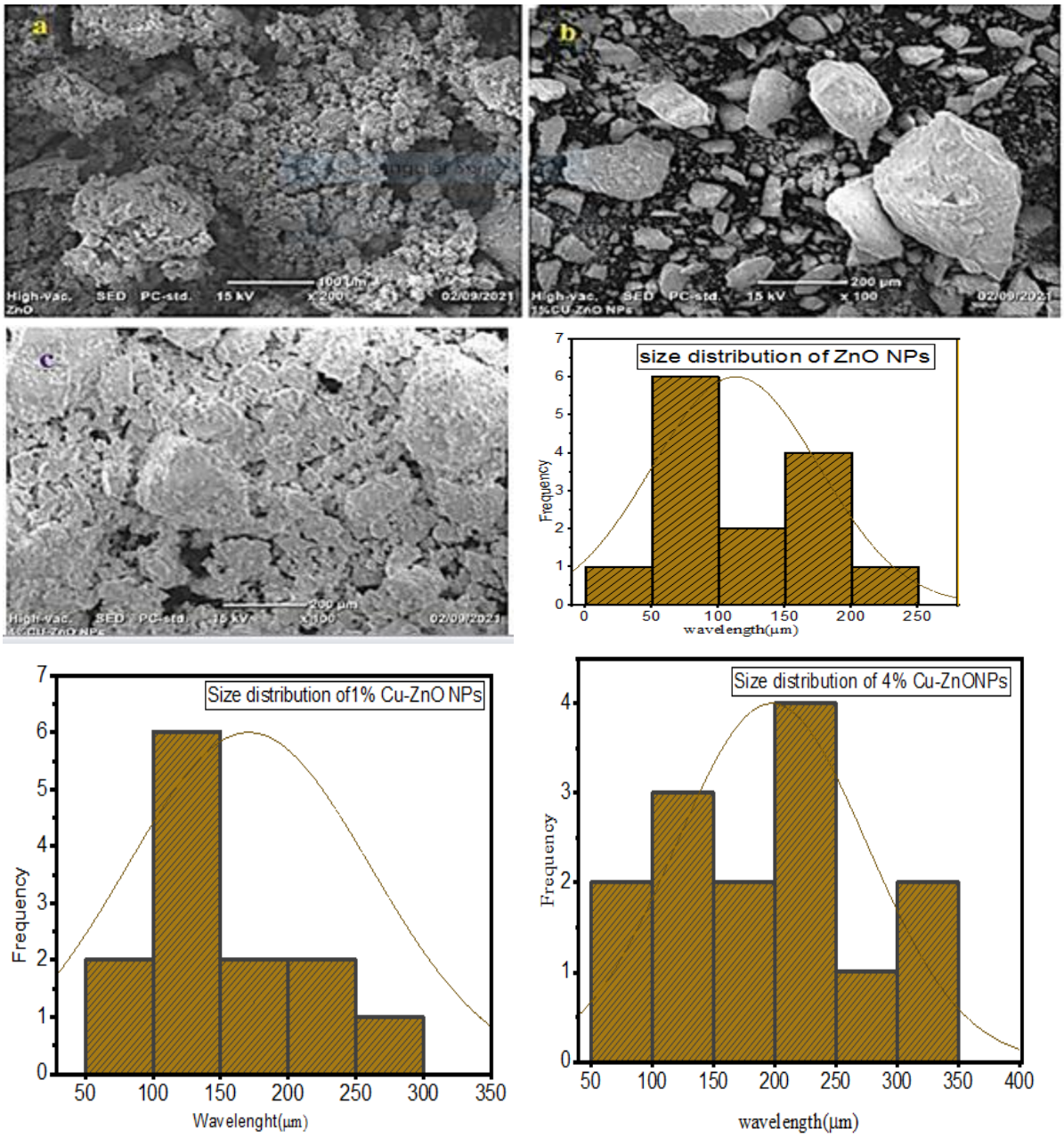

Figure 12: The SEM micrograph of: (a) ZnO sample. (b) 1% Cu-doped ZnO sample. (c) 4% Cu-doped ZnO NPs sample with their size distributions

4.4. Antibacterial activities of plant extract, ZnO and Cu-doped ZnO nanoparticles

The antibacterial activities of 100 µL plant extracted, ZnO, 1% Cu-doped ZnO, and 4% Cu-doped ZnO nanoparticles were tested against gram-positive bacteria (*Bacillus cereus* and *Staphylococcus aureus)* and gram negative bacteria (*Escherichia coli and Salmonella typhi)* using agar plate disc diffusion method [84]**.** The bacterial strains were obtained from the

Microbiology Laboratory, Biology Department, and Jimma University. As it shown in Table 5, the maximum zone inhibition activities were found against gram-positive (*B. cereus and S. aureus*) for 4% Cu-doped ZnO NPs followed by 1% Cu-doped ZnO NPs, whereas minimum inhibition zone were seen for gram-negative (*E.coli and S.typhi*). But no activity was seen for ZnO against both gram-positive and gram negative as well as for 1% Cu-doped ZnO NPs against E.coli. The antibacterial effect of Cu-doped ZnO was more pronounced for Gram-positive bacteria as compared to Gram-negative bacteria, which is on the basis of differences in (i) cell membrane structure, (ii) physiology and metabolic activities of the cell, and (iii) degree of contact of Gram-positive and Gram-negative bacteria [69].

The possible inhibitory action is physical damage caused by the interaction of the nanomaterial with the outer cell wall layer.

Table 5: Antibacterial activities with their inhibition zone of plant extract, ZnO and Cu-doped ZnO nanoparticles

Samples	Bacteria strain			
	Gram-positive		Gram-negative	
	B. cereus	S.aureas	E.coli	S.typhi
ZnO NPS	-	-	-	-
1 % Cu-doped ZnO NPs	10 mm	17 mm	-	14 mm
4% Cu-doped ZnO NPs	24 mm	25 mm	22 mm	22 mm
Gentamicin	18 mm	22 mm	24 mm	14 mm
DMSO	NI	NI	NI	NI
Plant extract	-	-	-	-

NI= No inhibit

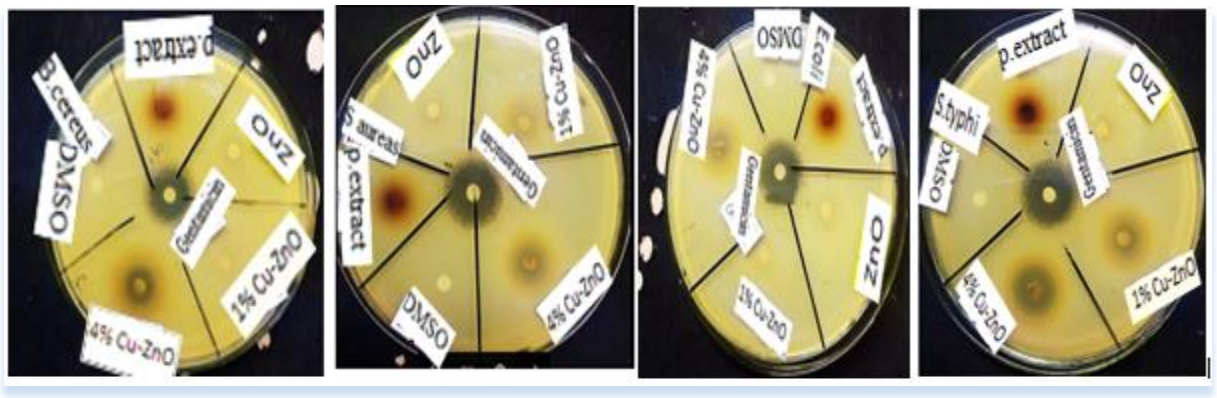

Figure 13 : Diameter of inhibition zones of all the samples against selected bacteria.

4.5. Photocatalytic activities

Four different photodegradation treatments of MB dye were conducted, namely UV photolysis (without catalyst), plant mediated green synthesized ZnO, 1% Cu-doped ZnO and 4% Cu-doped ZnO Nps. As a control treatment, photolysis was conducted by directly exposing the UV source to MB solution without the catalyst samples. Photocatalytic degradation of MB dye was conducted by exposing the UV light to the MB-photocatalyst suspension for the three catalysts. Dye degradation was visually detected by a gradual change in the color from deep blue to the colorless dye solution. The dye degradation in presence of biosynthesized, nanoparticles was verified by the decrease of the peak intensity at 665 nm during 180 min exposure under UV light irradiation.

Photolysis treatment did not result in a significant decrease of MB dye and was only able to degrade 15.73% of MB compounds during 180 min of UV irradiation. This is because the UV energy is not able to break the MB compound bonds quickly and optimally. The photocatalysis treatment was significant in the degradation of MB dye for all ZnO, 1% Cu-doped ZnO and 4% Cu-doped ZnO NPs. ZnO nanoparticles degrade 70% of MB which is similar result obtained by [85] , while 1% Cu-doped ZnO and 4% Cu-doped ZnO Nps degrade 78.48% and 88.07 % of MB respectively, indicating the enhancement of degradation efficiency with doping.

4.5.1. Effect of initial dye concentration

The effect of initial dye concentration on the degradation efficiency was studied at the optimum (pH= 10) and catalyst quantity (50 mg) by varying initial dye concentration. Different initial concentrations of MB in the range of 8-15 mg/L were used to assess the photocatalytic activity.

Figure 14 shows maximum degradation was observed at a dye concentration of 10 mg/L, because of enough dye molecules presence in comparison to $OH^{\bullet}$ radicals for the degradation of dye. For the initial dye concentration of 8 mg/L, the degradation values are found to be lower than that of 10 mg/L, because of the lower number of dye molecules present in the solution and lower utilization of $OH^{\bullet}$ radicals. When the concentration of MB increases, the PDE was decreased due to the fact that the available hydroxyl radicals for attacking MB molecules become less because more MB molecules are adsorbed on the surface of ZnO. But the number of $OH^{\bullet}$ and O^{2-} radicals formed on the surface of ZnO and the irradiation time is constant and also the absorption of photons by the photocatalyst decreases. It indicates that the photons get interrupted before they can reach the photocatalyst surface. Thus, the optimum dye concentration is found to be 10 mg/ L[86]

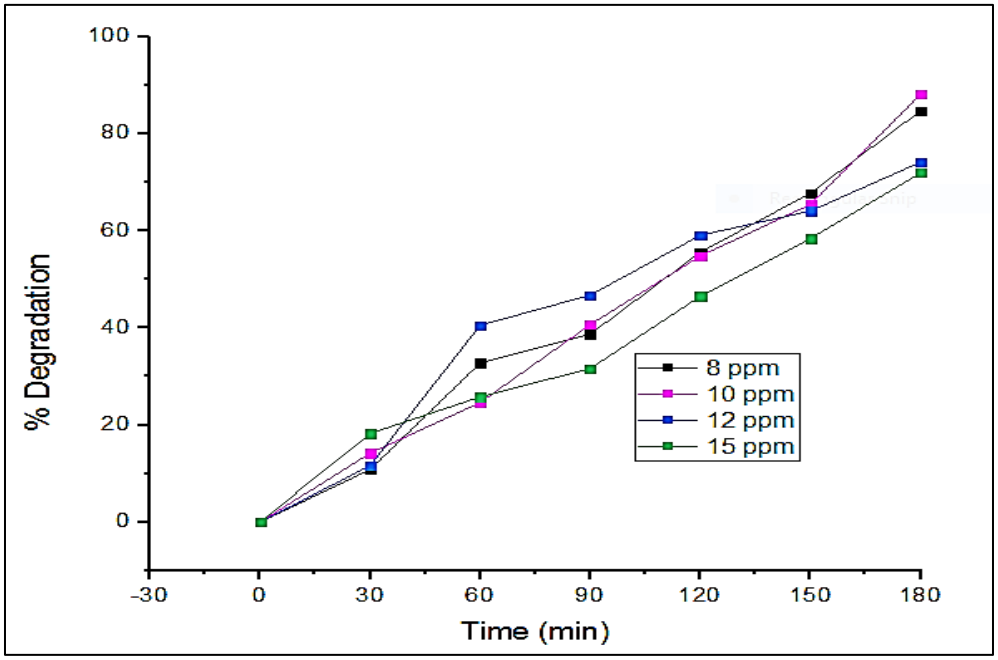

Figure 14: Photocatalytic effect at different a dye concentration

Table 6: Degradation efficiency for different concentration MB dye solution at pH=10 using 50 mg.

Dye concentration	8 ppm	10 ppm	12 ppm	15 ppm
Degradation efficiency in each dye concentration	84.7 %	88.03%	74%	71.9%

4.5.2. Effect of catalyst dose

The catalyst amounts were varied from 10 to 60 mg/100 mL. The degradation efficiency increases from 10 to 50 mg/100 mL, because the increase in catalyst amount increases the number of active sites on the photocatalyst surface. When the photocatalyst increased from 50 to 60 mg, the degradation efficiency decreased, because of the particle to particle interactions and light reflectance by catalyst particles. Similar results have been reported for the photodegradation of dyes by ZnO [87]. Thus optimum catalyst concentration for photocatalytic degradation of MB dye was taken as 50 mg.

Figure 15 shows the degradation spectra of methylene blue for the variation of catalytic load (10–60 mg) at constant dye concentration (10 ppm) and (pH=10). The data in Table 7 indicate that an increase in the catalytic load also increases degradation of dye from 69.37 % to 88.01% at the end of 180 min (Table 7). This is because the availability/concentration of active sites increases with the increase of catalytic amount.

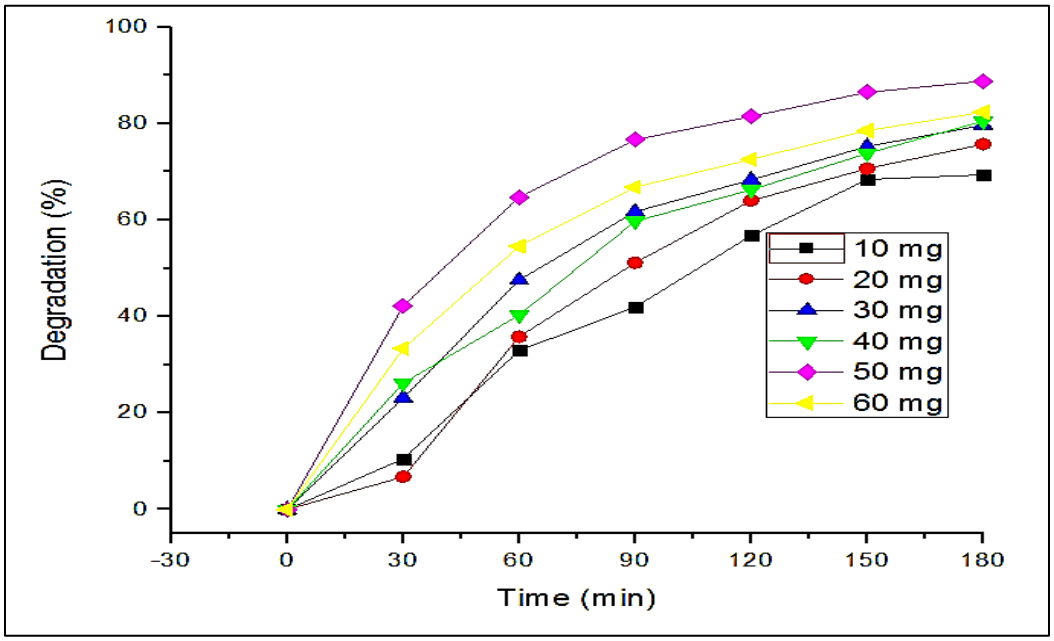

Figure 15 : Degradation spectra of methylene blue at different amount of catalyst

Table 7: Degradation efficiency of 10 ppm MB dye solution at different amount of catalyst at pH=10

Amount of catalyst	10 mg	20 mg	30 mg	40 mg	50 mg	60 mg
Degradation efficiency in each catalyst	69.37%	75.7%	79.6%	80.5%	88.01%	82.3%

4.5.3. Effect of pH

The pH of a solution is an important parameter for studying the photocatalytic activity of a catalyst as it provides information on the surface charge properties of the catalysts [86]. Figure 16 shows the photodegradation activity of, Cu-doped ZnO NPs sample on degrading 10 ppm of MB using 50 mg at pH vales of 4, 6, 8, 10, and 12. The degradation efficiency increases with the increase of pH. At acidic pH, the removal efficiency is less due to the dissolution of Cu-doped ZnO NPs and higher at alkaline pH values, due to production of hydroxyl radicals that results in higher photocatalytic degradation of methylene blue.

The zero point charge of Cu-doped ZnO is at pH-7. Above this pH value, Cu-doped ZnO surface is negatively charged and in aqueous solution, MB has positive charged. Due to electrostatic interaction between the negatively charged Cu-doped ZnO surface and positively charged MB dye, better photodegradation efficiency is obtained in alkaline solution. The photodegradation of MB increases from pH 4–10 and then decreases as the pH increases to 12. This is due to the change in electrostatic attraction or repulsion between dye molecules and catalysts. Thus optimum degradation of Methylene blue dye is obtained at pH-10 which degrades the dye up to 88.07 % under the irradiation time of 180 min.

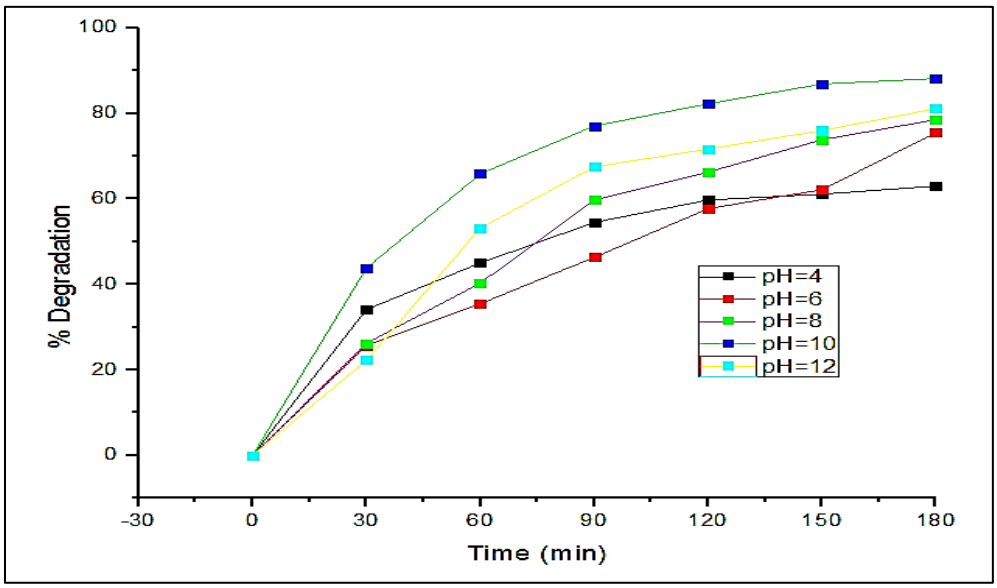

Figure 16: 10 ppm of initial MB dye solution maintained at different pH-values using 50 mg of Cu-doped ZnO NPs**.**

Table 8: Degradation efficiency for 10 ppm of initial MB dye solution maintained at different pH-values using 50 mg

pH values	4	6	8	10	12
Degradation efficiency in each pH values	63%	75%	78.5%	88.07%	81.03%

The mechanism of photocatalysis for Cu-doped ZnO nanoparticles has been illustrated in Figure 17. The photocatalysis process comprises (I) generation of electron–hole pair: The electron from the valence band gets excited to conduction band by absorbing UV light equal or higher than the band gap energy of catalyst. This leads to formation of holes in valence band and electrons excited to conduction band. Copper doping results in the formation of trap levels between the valence and conduction band of ZnO.

(II) separation of electron–hole pairs and (III) the electron- and hole-driven photo-redox reaction leads to the generation of highly active hydroxyl radical which is responsible for degradation of organic dyes [88].

Thus, Cu-doped ZnO nanoparticles effectively separate formed electron–hole pairs, forming more radicals and in turn enhancing the photocatalytic activity.

$$Cu–ZnO + h\upsilon \rightarrow Cu–ZnO\ (h^+ + e^-)$$

$$e^- + O_2 \rightarrow {}^{\bullet}O_2^-$$

$$h^+ + OH^- \rightarrow {}^{\bullet}OH$$

$${}^{\bullet}OH + \text{organic dye} \rightarrow \text{degradation products}$$

$${}^{\bullet}O_2^- + \text{organic dye} \rightarrow \text{degradation products}$$

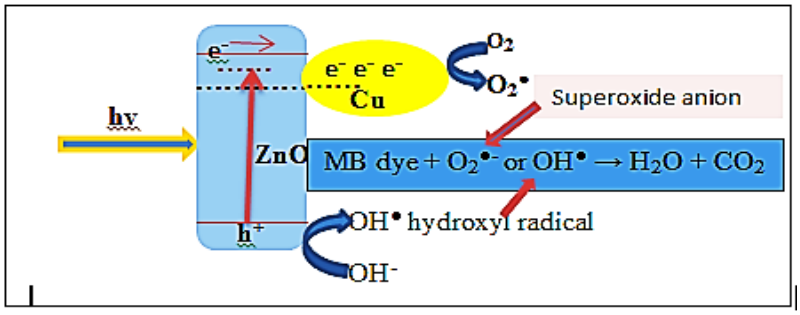

Figure 17 : The mechanism of photocatalysis for ZnO and Cu-doped ZnO NPs

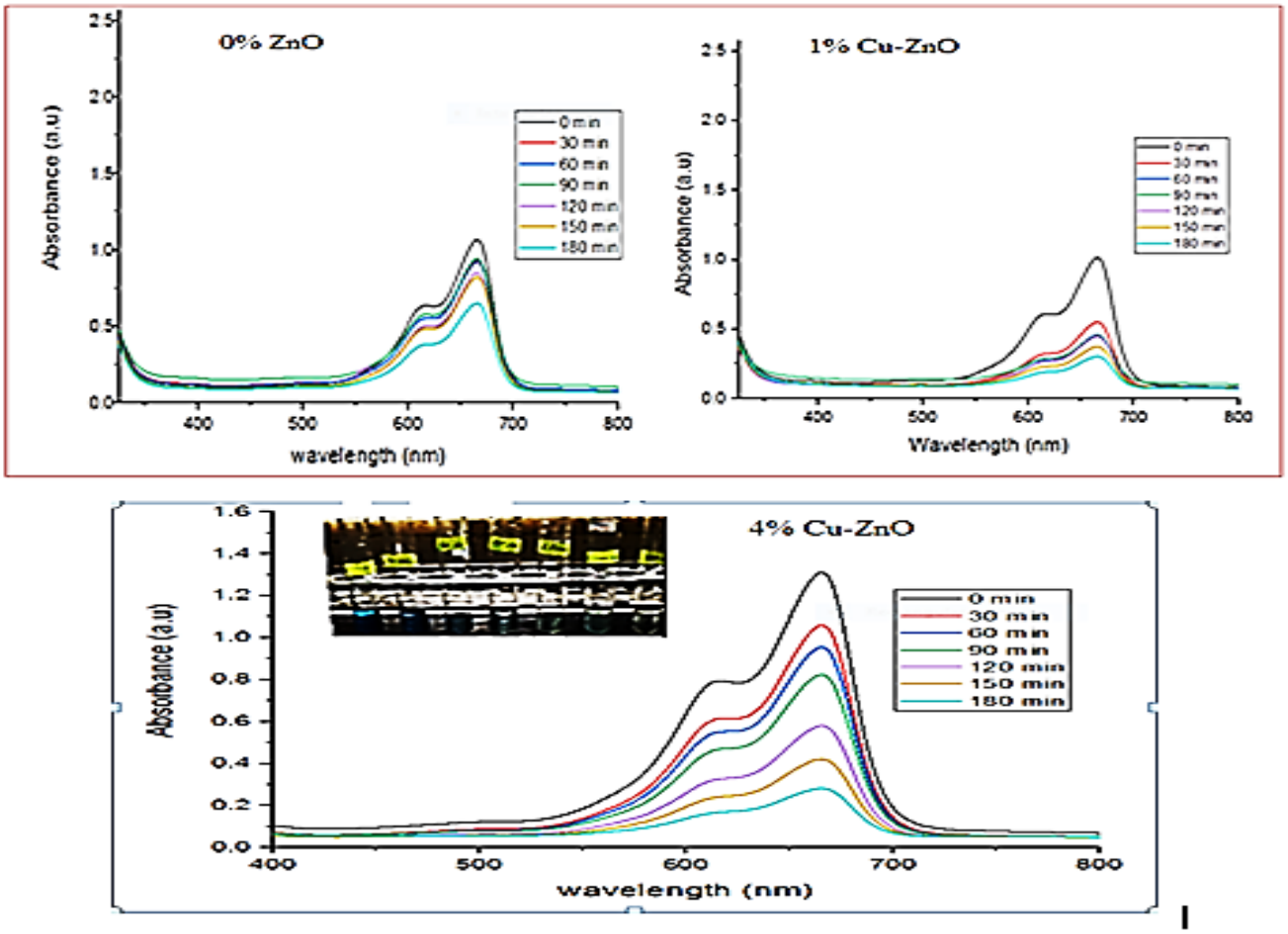

Figure 18 : Time dependent absorption spectra of MB dye in (a) 0% ZnO, (b) 1% Cu-ZnO, and (c) 4% Cu- ZnO NPs catalysts

4.6. Reusability of Cu–doped ZnO NPs

The reusability of the photocatalyst (4% Cu–doped ZnO) is also an important factor for practical applications and it was studied by recycling experiments. Photocatalytic experiments were performed under the optimum reaction conditions [pH = 10, MB concentration = 10 ppm, and catalyst dosage = 50 mg] using the same catalyst two times and the results are compiled in Figure 19. The photodegradation percentages of MB for the two successive cycling of Cu–doped ZnO NPs were 82.86 %, and 75.18 %, respectively. The slight decrease in the photocatalytic activity after two cycles is due to the accumulation of the adsorbed MB molecules on the catalyst surface. The results inferred that Cu–doped ZnO NPs is a reusable photocatalyst for the degradation of dyes.

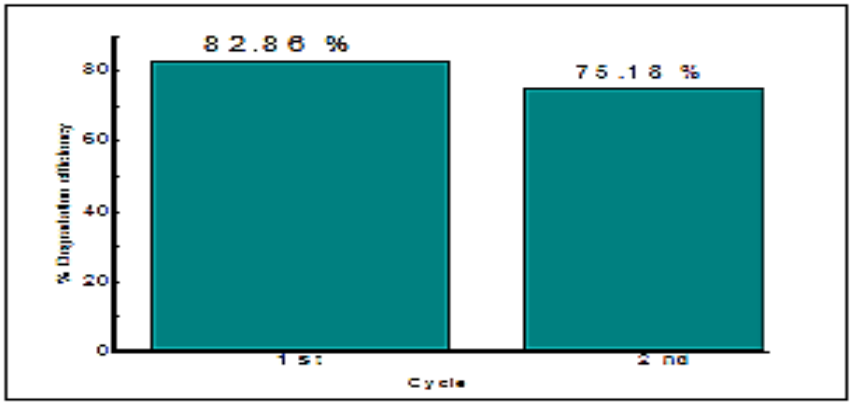

Figure 19: Reuse of Cu–doped ZnO NPs for the photodegradation of MB for two successive cycles

Table 9: Degradation efficiency of MB in the presence of photocatalyst under UV light irradiation

Catalysts	Dye concentration	Amount of catalyst	Degradation Time (min)	Degradation (%)	References
ZnO	15 ppm	200 mg	180	70	[85]
ZnO	10 ppm	10 mg	240	98	[89]
Al–Fe Co-doped ZnO	10 ppm	10 mg	75	90	[90]
ZnO	10 ppm	20 mg	200	80	[91]
ZnO	10 ppm	60 mg	120	100	[92]
ZnO	10 ppm	50 mg	180	70	Present work
4% Cu-doped ZnO	10 ppm	50 mg	180	88	Present work

5. CONCLUSION AND RECOMMENDATIONS

5.1. Conclusion

Aloe vera leaf extract was successfully used to synthesize ZnO, 1% Cu-doped ZnO and 4% Cu-doped ZnO NPs. The structural, morphological, nature of bond and optical properties of the samples were characterized using XRD, SEM, FT-IR, and UV-Visible spectroscopy. All the samples were crystalline in nature with wurtzite hexagonal structure and their crystallite size increased from 19.24 nm to 24.91 nm as Cu content increased from 0 to 4%. The energy band gap was found to decline from 3.17 to 2.83 eV as Cu concentration was raised from 0 to 4%. The FT-IR study revealed the presence of reducing, stabilizing, and capping phytochemicals present in *Aloe vera* leaf and the nanoparticles. SEM result revealed that the surface morphology of ZnO NPs altered with increase in Cu concentration. The antibacterial investigation showed that selected pathogens were sensitive to 1% Cu-doped ZnO and 4% Cu-doped ZnO NPs, however, 4% Cu-doped ZnO NPs showed better antibacterial activities across the selected pathogens. Photocatalytic activities of 1% Cu-doped ZnO and 4% Cu-doped ZnO NPs had better percentage degradation efficiency (78.48 and 88.07%) after 180 min of irradiation.

5.2. Recommendation

Since the green synthesis of Cu-doped ZnO NPs is better anti-bacterial activity, photocatalytic dye degradation, and more other applications, environmentally friendly and easy to handle, inexpensive to prepare.:-

- More attention must be given to carry out more researches on this area.
- Also additional characterization for further size determination, morphology and elemental composition of the sample using instruments; TEM and EDX.

6. REFERENCES

[1] Belisti Lelisa, M. M. Removal of Methylene Blue (Mb) Dye from Aqueous Solution by Bioadsorption onto Untreated Parthenium Hystrophorous Weed. *Mod. Chem. Appl.*, **2014**, *02* (04).

[2] Kahsay, M. H. Synthesis and Characterization of ZnO Nanoparticles Using Aqueous Extract of Becium Grandiflorum for Antimicrobial Activity and Adsorption of Methylene Blue. *Appl. Water Sci.*, **2021**, *11* (2), 1–12.

[3] Verma, R. K. Eradication of Fatal Textile Industrial Dyes by Wastewater Treatment. *Biointerface Res. Appl. Chem.*, **2021**, *12* (1), 567–587.

[4] Mohammad Mostafa. Waste Water Treatment in Textile Industries-the Concept and Current Removal Technologies Mohammad Mostafa. *J. Biodivers. Environ. Sci.*, **2016**.

[5] Nagar, N. Synthesis of Metal Nanoparticles and Their Application in Degradation of Textile Dyes by Advanced Oxidation Process.

[6] Ghaffar, A.; Zhang, L.; Zhu, X.; Chen, B. Porous PVdF/GO Nanofibrous Membranes for Selective Separation and Recycling of Charged Organic Dyes from Water. *Environ. Sci. Technol.*, **2018**, *52* (7), 4265–4274.

[7] Sharma, A.; Ahmad, J.; Flora, S. J. S. Application of Advanced Oxidation Processes and Toxicity Assessment of Transformation Products. *Environ. Res.*, **2018**, *167* (March), 223–233.

[8] Alalm, M. G.; Djellabi, R.; Meroni, D.; Pirola, C.; Bianchi, C. L.; Boffito, D. C. Toward Scaling-up Photocatalytic Process for Multiphase Environmental Applications. *Catalysts*, **2021**, *11* (5), 1–23.

[9] Pal, S.; Mondal, S.; Maity, J.; Mukherjee, R. Synthesis and Characterization of Zno Nanoparticles Using Moringa Oleifera Leaf Extract: Investigation of Photocatalytic and Antibacterial Activity. *Int. J. Nanosci. Nanotechnol.*, **2018**, *14* (2), 111–119.

[10] Branch, V. P. Department of Chemistry, Science and Research Branch, Islamic Azad University, Tehran, Iran. Department of Chemistry, Azarbaijan Shahid Madani University, Tabriz, Iran. 3 Department of Chemistry, Payame Noor University, Tehran, Iran. 4 Department of Chemi. **2020**, No. January, 32–35.

[11] Aneesh, P. M.; Vanaja, K. A.; Jayaraj, M. K. Synthesis of ZnO Nanoparticles by Hydrothermal Method. *Nanophotonic Mater. IV*, **2007**, *6639* (September 2007).

[12] Cui, Y.; Lieber, C. M. Linked References Are Available on JSTOR for This Article : Functional Nanoscale Electronic Devices Assembled Using Silicon Nanowire Building Blocks. **2017**, *291* (5505), 851–853.

[13] Singh, S.; Srivastava, V. C.; Lo, S. L.; Mandal, T. K.; Naresh, G. Morphology-Controlled Green Approach for Synthesizing the Hierarchical Self-Assembled 3D Porous ZnO Superstructure with Excellent Catalytic Activity. *Microporous Mesoporous Mater.*, **2017**, *239*, 296–309.

[14] Ahmad, M.; Pan, C.; Yan, W.; Zhu, J. Effect of Pb-Doping on the Morphology, Structural and Optical Properties of ZnO Nanowires Synthesized via Modified Thermal Evaporation. *Mater. Sci. Eng. B Solid-State Mater. Adv. Technol.*, **2010**, *174* (1–3), 55–58.

[15] Gwizdz, P.; Lyson-Sypien, B.; Radecka, M.; Rekas, M.; Zakrzewska, K. Response Modeling of Temperature Modulated Array of Chromium Doped Nanostructured TiO_2 Gas Sensors. *Procedia Eng.*, **2015**, *120* (February 2016), 1054–1057.

[16] Samadi, M.; Zirak, M.; Naseri, A.; Khorashadizade, E.; Moshfegh, A. Z. Recent Progress on Doped ZnO Nanostructures for Visible-Light Photocatalysis. *Thin Solid Films*, **2016**, *605*, 2–19.

[17] Cao, F. F.; Xin, S.; Guo, Y. G.; Wan, L. J. Wet Chemical Synthesis of Cu/TiO_2 Nanocomposites with Integrated Nano-Current-Collectors as High-Rate Anode Materials in Lithium-Ion Batteries. *Phys. Chem. Chem. Phys.*, **2011**, *13* (6), 2014–2020.

[18] Kathiresan, K.; Manivannan, S.; Nabeel, M. A.; Dhivya, B. Studies on Silver Nanoparticles Synthesized by a Marine Fungus, Penicillium Fellutanum Isolated from Coastal Mangrove Sediment. *Colloids Surfaces B Biointerfaces*, **2009**, *71* (1), 133–137.

[19] Lakshmeesha, T. R.; Sateesh, M. K.; Prasad, B. D.; Sharma, S. C.; Kavyashree, D.; Chandrasekhar, M.; Nagabhushana, H. Reactivity of Crystalline ZnO Superstructures against Fungi and Bacterial Pathogens : Synthesized Using Nerium Oleander Leaf Extract. **2014**.

[20] Siddiqi, K. S.; Husen, A. Recent Advances in Plant-Mediated Engineered Gold Nanoparticles and Their Application in Biological System. *J. Trace Elem. Med. Biol.*, **2017**, *40*, 10–23.

[21] Arunkumar, S.; Muthuselvam, M. Analysis of Phytochemical Constituents and Antimicrobial Activities of Aloe Vera L. against Clinical Pathogens. *World J. Agric. Sci.*,

2009, *5* (5), 572–576.

[22] Jafarirad, S.; Mehrabi, M.; Divband, B.; Kosari-nasab, A. Mechanistic Approach Biofabrication of Zinc Oxide Nanoparticles Using Fruit Extract of Rosa Canina and Their Toxic Potential Again. *Mater. Sci. Eng. C*, **2015**, *59* (March 2018), 296–302.

[23] Shoeb, E.; Hefferon, K. Future of Cancer Immunotherapy Using Plant Virus-Based Nanoparticles. **2019**, *5*.

[24] Uskoković, V. Nanomaterials and Nanotechnologies : Approaching the Crest of This Big Wave Nanomaterials and Nanotechnologies : *Approaching the Crest of This Big*. **2008**, *4* (2), 119–129.

[25] Fageria, P.; Gangopadhyay, S.; Pande, S. figure S. of Z. and Z. N. and T. P. A. U. U. and V. L. A. simple approach for the deposition of A. and A. nanoparticles on Z. surface and investigate their. T Application in Pollutant Degradation.

[26] Mahendiran, D.; Subash, G.; Selvan, D. A.; Rehana, D. Biosynthesis of Zinc Oxide Nanoparticles Using Plant Extracts of Aloe Vera and Hibiscus Sabdariffa : Phytochemical , Antibacterial , Antioxidant and Anti-Proliferative Studies. **2017**.

[27] Jadoun, S.; Arif, R.; Jangid, N. K.; Meena, R. K. Green Synthesis of Nanoparticles Using Plant Extracts: A Review. *Environ. Chem. Lett.*, **2021**, *19* (1), 355–374.

[28] Kulkarni, M. B.; Goel, S. Microfluidic Devices for Synthesizing Nanomaterials—a Review. *Nano Express*, **2020**, *1* (3), 032004.

[29] Chai, H.; Lam, S.; Sin, J. Green Synthesis of Magnetic Fe-Doped ZnO Nanoparticles via Hibiscus Rosa-Sinensis Leaf Extracts for Boosted Photocatalytic , Antibacterial and Antifungal Activities. *Mater. Lett.*, **2019**, *242*, 103–106.

[30] Minwuyelet, T.; Sewalem, M.; Gashe, M. Review on Therapeutic Uses of Aloe Vera. **2017**, *11* (2), 14–20.

[31] Manzoor, U.; Tuz Zahra, F.; Rafique, S.; Moin, M. T.; Mujahid, M. Effect of Synthesis Temperature, Nucleation Time, and Postsynthesis Heat Treatment of ZnO Nanoparticles and Its Sensing Properties. *J. Nanomater.*, **2015**, *2015*.

[32] Agarwal, H.; Venkat Kumar, S.; Rajeshkumar, S. A Review on Green Synthesis of Zinc Oxide Nanoparticles – An Eco-Friendly Approach. *Resour. Technol.*, **2017**, *3* (4), 406–413.

[33] Chandrasekaran, R.; Gnanasekar, S.; Seetharaman, P.; Keppanan, R.; Arockiaswamy, W.;

Sivaperumal, S. Formulation of Carica Papaya Latex-Functionalized Silver Nanoparticles for Its Improved Antibacterial and Anticancer Applications. *J. Mol. Liq.*, **2016**, *219*, 232–238.

[34] Musleh, H.; AlDahoudi, N.; Zayed, H.; Shaat, S.; Tamous, H. M.; Shurrab, N.; Issa, A.; Asad, J. Synthesis and Characterization of Zno Nanoparticles Using Hydrothermal and Sol-Gel Techniques for Dye-Sensitized Solar Cells. *J. Univ. Babylon Eng. Sci.*, **2018**, *26* (9), 256–267.

[35] Naveed Ul Haq, A.; Nadhman, A.; Ullah, I.; Mustafa, G.; Yasinzai, M.; Khan, I. Synthesis Approaches of Zinc Oxide Nanoparticles: The Dilemma of Ecotoxicity. *J. Nanomater.*, **2017**, *2017*.

[36] Sahai, A.; Goswami, N. Structural and Optical Investigations of Oxygen Defects in Zinc Oxide Nanoparticles. *AIP Conf. Proc.*, **2015**, *1665* (December).

[37] Jeevanandam, J.; Chan, Y. S.; Danquah, M. K. Biosynthesis of Metal and Metal Oxide Nanoparticles. *ChemBioEng Rev.*, **2016**, *3* (2), 55–67.

[38] Guldiken, B.; Ozkan, G.; Catalkaya, G.; Ceylan, F. D.; Ekin Yalcinkaya, I.; Capanoglu, E. Phytochemicals of Herbs and Spices: Health versus Toxicological Effects. *Food Chem. Toxicol.*, **2018**, *119* (May), 37–49.

[39] Mittal, A. K.; Chisti, Y.; Banerjee, U. C. Synthesis of Metallic Nanoparticles Using Plant Extracts. *Biotechnol. Adv.*, **2013**, *31* (2), 346–356.

[40] Altemimi, A.; Lakhssassi, N.; Baharlouei, A.; Watson, D. G.; Lightfoot, D. A. Phytochemicals: Extraction, Isolation, and Identification of Bioactive Compounds from Plant Extracts. *Plants*, **2017**, *6* (4).

[41] Folorunso, A.; Akintelu, S.; Oyebamiji, A. K.; Ajayi, S.; Abiola, B.; Abdusalam, I.; Morakinyo, A. Biosynthesis, Characterization and Antimicrobial Activity of Gold Nanoparticles from Leaf Extracts of Annona Muricata. *J. Nanostructure Chem.*, **2019**, *9* (2), 111–117.

[42] Fagier, M. A. Plant-Mediated Biosynthesis and Photocatalysis Activities of Zinc Oxide Nanoparticles : A Prospect towards Dyes Mineralization. **2021**, *2021*.

[43] Jaffri, S. B.; Ahmad, K. S. Foliar-Mediated Ag:ZnO Nanophotocatalysts: Green Synthesis, Characterization, Pollutants Degradation, and in Vitro Biocidal Activity. *Green Process. Synth.*, **2019**, *8* (1), 172–182.

[44] Avis, A.; Babu, T.; Antony, R. Green Synthesis of Silver Doped Nano Metal Oxides of Zinc & Copper for Antibacterial Properties, Adsorption, Catalytic Hydrogenation & Photodegradation of Aromatics. *Biochem. Pharmacol.*, **2018**.

[45] Chan, Y. Y.; Pang, Y. L.; Lim, S.; Chong, W. C. Facile Green Synthesis of ZnO Nanoparticles Using Natural-Based Materials: Properties, Mechanism, Surface Modification and Application. *J. Environ. Chem. Eng.*, **2021**, *9* (4), 105417.

[46] Ahmad, S.; Noreen, F.; Kanwal, S.; Iqbal, A.; Hussain, G. Materials Science & Engineering C Green Synthesis of ZnO and Cu-Doped ZnO Nanoparticles from Leaf Extracts of Abutilon Indicum , Clerodendrum Infortunatum , Clerodendrum Inerme and Investigation of Their Biological and Photocatalytic Activities. *Mater. Sci. Eng. C*, **2018**, *82* (August 2017), 46–59.

[47] Nagasundari, S. M.; Muthu, K.; Kaviyarasu, K.; Al, D. A. Current Trends of Silver Doped Zinc Oxide Nanowires Photocatalytic Degradation for Energy and Environmental Application. *Surfaces and Interfaces*, **2021**, *23* (January).

[48] Khan, M. I.; Fatima, N.; Shakil, M.; Tahir, M. B.; Riaz, K. N.; Rafique, M.; Iqbal, T.; Mahmood, K. Investigation of In-Vitro Antibacterial and Seed Germination Properties of Green Synthesized Pure and Nickel Doped ZnO Nanoparticles. *Phys. B Condens. Matter*, **2021**, *601* (February 2021).

[49] Synthesis, G.; Zinc, O. F.; Nanoparticles, O.; Peel, P.; Of, D.; Mill, T.; Activity, B. Y. P. Green Synthesis Of Zinc Oxide Nanoparticles Using Potato Peel And Degradation Of Textile Mill Effluent. **2017**, *6* (6), 774–785.

[50] Chauhan, A.; Verma, R.; Kumari, S.; Sharma, A.; Shandilya, P.; Li, X.; Batoo, K. M.; Imran, A.; Kulshrestha, S.; Kumar, R. Photocatalytic Dye Degradation and Antimicrobial Activities of Pure and Ag-Doped ZnO Using Cannabis Sativa Leaf Extract. *Sci. Rep.*, **2020**, *10* (1), 1–16.

[51] Jha, A.; Prakash, D.; Bisht, D. A Phytochemical Screening of the Ethanolic Extract of Aloe Vera Gel. **2019**, *8* (10), 2018–2020.

[52] Gavade, N. L.; Kadam, A. N.; Babar, S. B.; Gophane, A. D.; Garadkar, K. M.; Lee, S. W. Biogenic Synthesis of Gold-Anchored ZnO Nanorods as Photocatalyst for Sunlight-Induced Degradation of Dye Effluent and Its Toxicity Assessment. *Ceram. Int.*, **2020**, *46* (8), 11317–11327.

[53] Brintha, S. R.; Ajitha, M. Synthesis and Characterization of ZnO Nanoparticles via Aqueous Solution, Sol-Gel and Hydrothermal Methods. *IOSR J. Appl. Chem.*, **2015**, *8* (11), 66–72.

[54] Thakur, S.; Kumar, J.; Sharma, J.; Sharma, N.; Kumar, P. Structural and Optical Study of Nickel Doped ZnO Nanoparticles and Thin Films for Dye Sensitized Solar Cell Applications. *J. Optoelectron. Adv. Mater.*, **2013**, *15* (9–10), 989–994.

[55] Khalid, U. B. Optical Properties of Sb Doped ZnO Grown by VLS In Partial Fulfillment of the Requirement. **2015**.

[56] Bai, X.; Li, L.; Liu, H.; Tan, L.; Liu, T.; Meng, X. Solvothermal Synthesis of ZnO Nanoparticles and Anti-Infection Application in Vivo. *ACS Appl. Mater. Interfaces*, **2015**, *7* (2), 1308–1317.

[57] Pratap Goutam, S.; Kumar Yadav, A.; Jyoti Das, A. Coriander Extract Mediated Green Synthesis of Zinc Oxide Nanoparticles and Their Structural , Optical and Antibacterial ... *J. Nanosci. Technol.*, **2017**, *3* (October), 249–252.

[58] Search, H.; Journals, C.; Contact, A.; Iopscience, M.; Conf, I. O. P.; Address, I. P. Antimicrobial Property of Zinc Based Nanoparticles. *012055*.

[59] Umar, M.; Abdul Aziz, H. Photocatalytic Degradation of Organic Pollutants in Water by Polyoxometalates. *Org. Pollut. -Monitoring, Risk Treat.*, **2013**, 195–208.

[60] Kowsari, E. Carbon-Based Nanocomposites for Visible Light-Induced Photocatalysis. **2017**, 203–249.

[61] Haque, M. J.; Bellah, M. M.; Hassan, M. R.; Rahman, S. Synthesis of ZnO Nanoparticles by Two Different Methods & Comparison of Their Structural, Antibacterial, Photocatalytic and Optical Properties. *Nano Express*, **2020**, *1* (1).

[62] Hemalatha, P.; Karthick, S. N.; Hemalatha, K. V.; Yi, M.; Kim, H. J.; Alagar, M. La-Doped ZnO Nanoflower as Photocatalyst for Methylene Blue Dye Degradation under UV Irradiation. *J. Mater. Sci. Mater. Electron.*, **2016**, *27* (3), 2367–2378.

[63] Of, S.; Oxide, Z.; Using, N.; Extracts, L. A. Synthesis Of Zinc Oxide Nanoparticles Using Aloe Vera Leaf Aqueous Extracts And Its. **2019**, *Xvii* (1).

[64] Roopalatha, U. C.; Mala Nair, V. Phytochemical Analysis of Successive Reextracts of the Leaves of Moringa Oleifera Lam. *Int. J. Pharm. Pharm. Sci.*, **2013**, *5* (SUPPL 3), 629–634.

[65] Senthilkumar, N.; Nandhakumar, E.; Priya, P.; Soni, D.; Vimalan, M.; Vetha Potheher, I. Synthesis of ZnO Nanoparticles Using Leaf Extract of: Tectona Grandis (L.) and Their Anti-Bacterial, Anti-Arthritic, Anti-Oxidant and in Vitro Cytotoxicity Activities. *New J. Chem.*, **2017**, *41* (18), 10347–10356.

[66] Satisfaction, O. C.; Kumar, V. ISSN NO : 0042-9945 Volume XI , Issue II , February / 2020 Page No : 280 ISSN NO : 0042-9945 Page No : 281. **2020**, *XI* (280), 280–324.

[67] Khan, M. M.; Harunsani, M. H.; Tan, A. L.; Hojamberdiev, M.; Poi, Y. A.; Ahmad, N. Antibacterial Studies of ZnO and Cu-Doped ZnO Nanoparticles Synthesized Using Aqueous Leaf Extract of Stachytarpheta Jamaicensis. *Bionanoscience*, **2020**, *10* (4), 1037–1048.

[68] Bakht, J.; Islam, A.; Ali, H.; Tayyab, M.; Shafi, M. Antimicrobial Potentials of Eclipta Alba by Disc Diffusion Method. **2011**, *10* (39), 7658–7667.

[69] Bhuyan, T.; Mishra, K.; Khanuja, M.; Prasad, R.; Varma, A. Biosynthesis of Zinc Oxide Nanoparticles from Azadirachta Indica for Antibacterial and Photocatalytic Applications. *Mater. Sci. Semicond. Process.*, **2015**, *32*, 55–61.

[70] M. Elmorsi, T. M.; Elsayed, M. H.; F. Bakr, M. Na Doped ZnO Nanoparticles Assisted Photocatalytic Degradation of Congo Red Dye Using Solar Light. *Am. J. Chem.*, **2017**, *7* (2), 48–57.

[71] Nazar, N.; Bibi, I.; Kamal, S.; Iqbal, M.; Nouren, S.; Jilani, K.; Umair, M.; Ata, S. Cu Nanoparticles Synthesis Using Biological Molecule of P. Granatum Seeds Extract as Reducing and Capping Agent: Growth Mechanism and Photo-Catalytic Activity. *Int. J. Biol. Macromol.*, **2018**, *106*, 1203–1210.

[72] Hebeish, A.; El-Shafei, A.; Sharaf, S.; Zaghloul, S. Novel Precursors for Green Synthesis and Application of Silver Nanoparticles in the Realm of Cotton Finishing. *Carbohydr. Polym.*, **2011**, *84* (1), 605–613.

[73] Hashemi, S.; Asrar, Z.; Pourseyedi, S.; Nadernejad, N. Green Synthesis of ZnO Nanoparticles by Olive (Olea Europaea). *IET Nanobiotechnology*, **2016**, *10* (6), 400–404.

[74] Khalil, M. M. H.; Ismail, E. H.; El-Baghdady, K. Z.; Mohamed, D. Green Synthesis of Silver Nanoparticles Using Olive Leaf Extract and Its Antibacterial Activity. *Arab. J. Chem.*, **2014**, *7* (6), 1131–1139.

[75] Poojary, M. M.; Passamonti, P.; Adhikari, A. V. Green Synthesis of Silver and Gold

Nanoparticles Using Root Bark Extract of Mammea Suriga: Characterization, Process Optimization, and Their Antibacterial Activity. *Bionanoscience*, **2016**, *6* (2), 110–120.

[76] R, M. C. R.; Rajalaxshmi, A. Green Synthesis , Characterization of ZnO Nanoparticles and Ceion Doped ZnO Nanoparticles Assisted Sesbania Grandiflora for Photocatalytic Application. **2016**, *4* (2), 1–6.

[77] Shahpal, A.; Choudhary, M. A.; Ahmad, Z. An Investigation on the Synthesis and Catalytic Activities of Pure and Cu-Doped Zinc Oxide Nanoparticles. *Cogent Chem.*, **2017**, *280*.

[78] Mittal, M.; Sharma, M.; Pandey, O. P. UV-Visible Light Induced Photocatalytic Studies of Cu Doped ZnO Nanoparticles Prepared by Co-Precipitation Method. *Sol. Energy*, **2014**, *110*, 386–397.

[79] S, G.; Belay, A.; Reddy AR, C.; Z, B. Synthesis and Characterizations of Zinc Oxide Nanoparticles for Antibacterial Applications. *J. Nanomed. Nanotechnol.*, **2017**, *s8* (December 2017).

[80] Karthik, K. V.; Raghu, A. V.; Reddy, K. R.; Ravishankar, R.; Sangeeta, M.; Shetti, N. P.; Reddy, C. V. Green Synthesis of Cu-Doped ZnO Nanoparticles and Its Application for the Photocatalytic Degradation of Hazardous Organic Pollutants. *Chemosphere*, **2022**, *287* (P2).

[81] Okeke, I.; Agwu, K.; Ubachukwu, A.; Maaza, M.; Ezema, F. Impact of Cu Doping on ZnO Nanoparticles Phyto-Chemically Synthesized for Improved Antibacterial and Photocatalytic Activities. *J. Nanoparticle Res.*, **2020**, *22* (9).

[82] Singhal, S.; Kaur, J.; Namgyal, T.; Sharma, R. Cu-Doped ZnO Nanoparticles: Synthesis, Structural and Electrical Properties. *Phys. B Condens. Matter*, **2012**, *407* (8), 1223–1226.

[83] Muthukumaran, S.; Gopalakrishnan, R. Structural, FTIR and Photoluminescence Studies of Cu Doped ZnO Nanopowders by Co-Precipitation Method. *Opt. Mater. (Amst).*, **2012**, *34* (11), 1946–1953.

[84] Zhao, B.; Deng, S.; Li, J.; Sun, C.; Fu, Y.; Liu, Z. Green Synthesis , Characterization and Antibacterial Study on the Catechin-Functionalized ZnO Nanoclusters Green Synthesis , Characterization and Antibacterial Study on the Catechin-Functionalized ZnO Nanoclusters. **2021**.

[85] Luque, P. A.; Nava, O.; Soto-Robles, C. A.; Vilchis-Nestor, A. R.; Garrafa-Galvez, H. E.;

Castro-Beltran, A. Effects of Daucus Carota Extract Used in Green Synthesis of Zinc Oxide Nanoparticles. *J. Mater. Sci. Mater. Electron.*, **2018**, *29* (20), 17638–17643.

[86] Anju Chanu, L.; Joychandra Singh, W.; Jugeshwar Singh, K.; Nomita Devi, K. Effect of Operational Parameters on the Photocatalytic Degradation of Methylene Blue Dye Solution Using Manganese Doped ZnO Nanoparticles. *Results Phys.*, **2019**, *12* (December 2018), 1230–1237.

[87] Pardeshi, S. K.; Patil, A. B. Effect of Morphology and Crystallite Size on Solar Photocatalytic Activity of Zinc Oxide Synthesized by Solution Free Mechanochemical Method. *J. Mol. Catal. A Chem.*, **2009**, *308* (1–2), 32–40.

[88] Arsana, P.; Bubpa, C.; Sang-aroon, W. Photocatalytic Activity under Solar Irradiation of Silver and Copper Doped Zincoxide: Photodeposition versus Liquid Impregnation Methods. *J. Appl. Sci.*, **2012**, *12* (17), 1809–1816.

[89] Raheem, Z.; Fouad, R. Preparation of ZnO for Photocatalytic Activity of Methylene Blue Dye Preparation of ZnO for Photocatalytic Activity of Methylene Blue Dye. **2017**.

[90] Hammad, A.; Khalid, N. R.; Hammad, A.; Tahir, M. B.; Ra, M.; Iqbal, T.; Nabi, G.; Hussain, M. K. Enhanced Photocatalytic Activity of Al and Fe Co-Doped ZnO Nanorods for Methylene Blue Degradation. *Ceram. Int.*, **2019**, No. October, 0–1.

[91] Alamdari, S.; Ghamsari, M. S.; Lee, C.; Han, W.; Park, H.; Tafreshi, M. J.; Afarideh, H. Applied Sciences Preparation and Characterization of Zinc Oxide Nanoparticles Using Leaf Extract of Sambucus Ebulus. 1–19.

[92] Madan, H. R.; Sharma, S. C.; Udayabhanu; Suresh, D.; Vidya, Y. S.; Nagabhushana, H.; Rajanaik, H.; Anantharaju, K. S.; Prashantha, S. C.; Sadananda Maiya, P. Facile Green Fabrication of Nanostructure ZnO Plates, Bullets, Flower, Prismatic Tip, Closed Pine Cone: Their Antibacterial, Antioxidant, Photoluminescent and Photocatalytic Properties. *Spectrochim. Acta - Part A Mol. Biomol. Spectrosc.*, **2016**, *152* (October 2018), 404–416.

APPENDICES

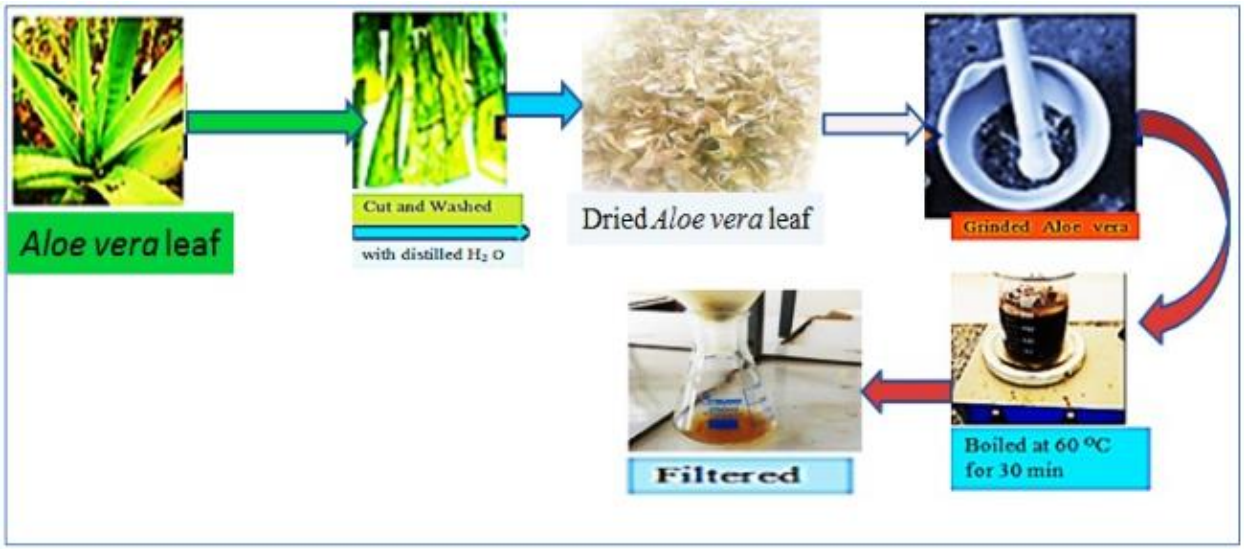

.

Appendix 1: schematic diagram for preparation of *Aloe vera* leaf Extract.

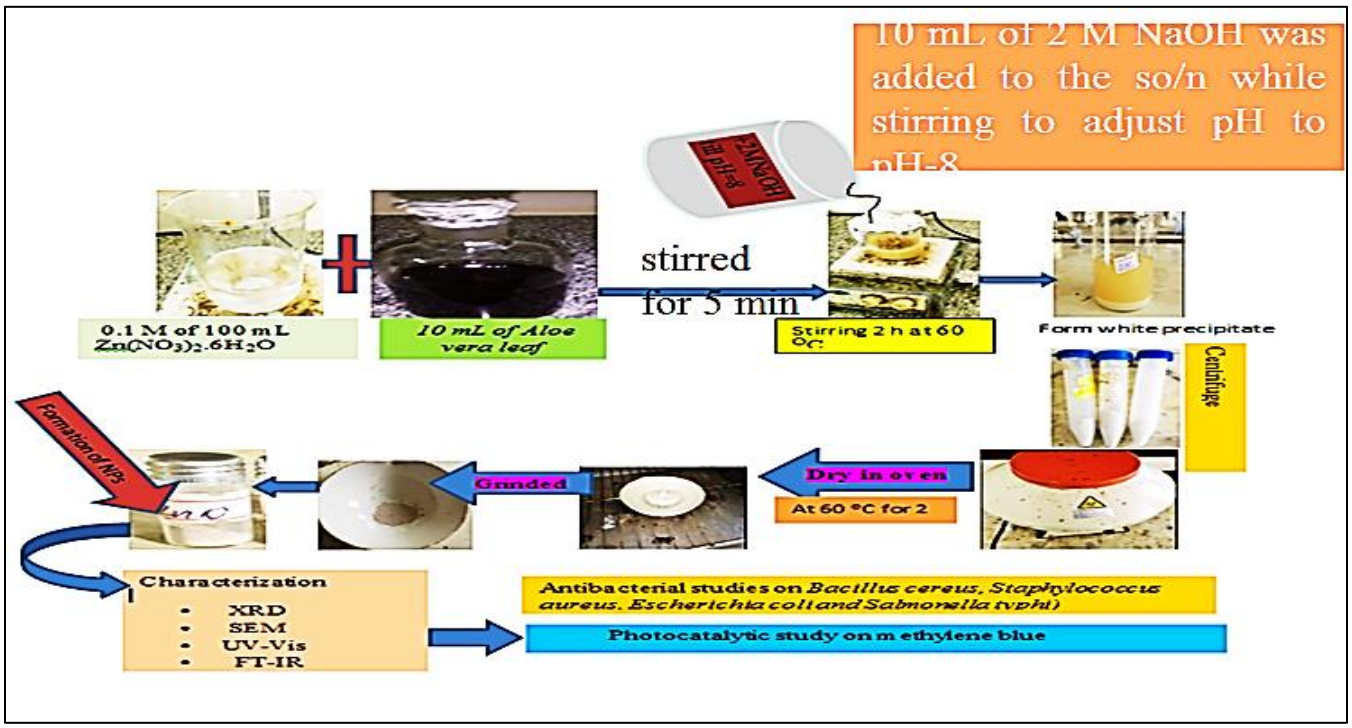

Appendix 2: schematic diagram for synthesis of ZnO NPs using Zinc nitrate hexahydrate and *Aloe vera* leaf Extract

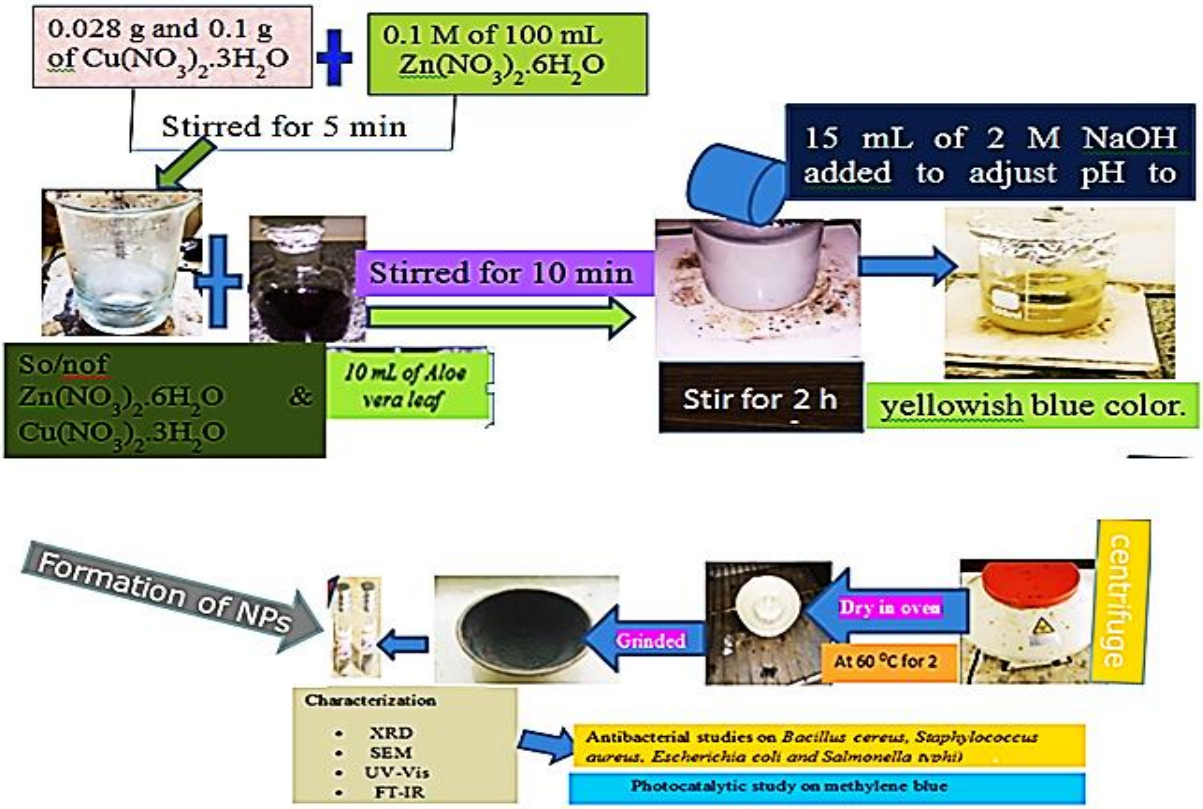

Appendix 3 **:** schematic diagram for synthesis 1% Cu-doped ZnO and 4% Cu-doped ZnO NPs using Zinc nitrate hexahydrate and *Aloe vera* leaf Extract

.

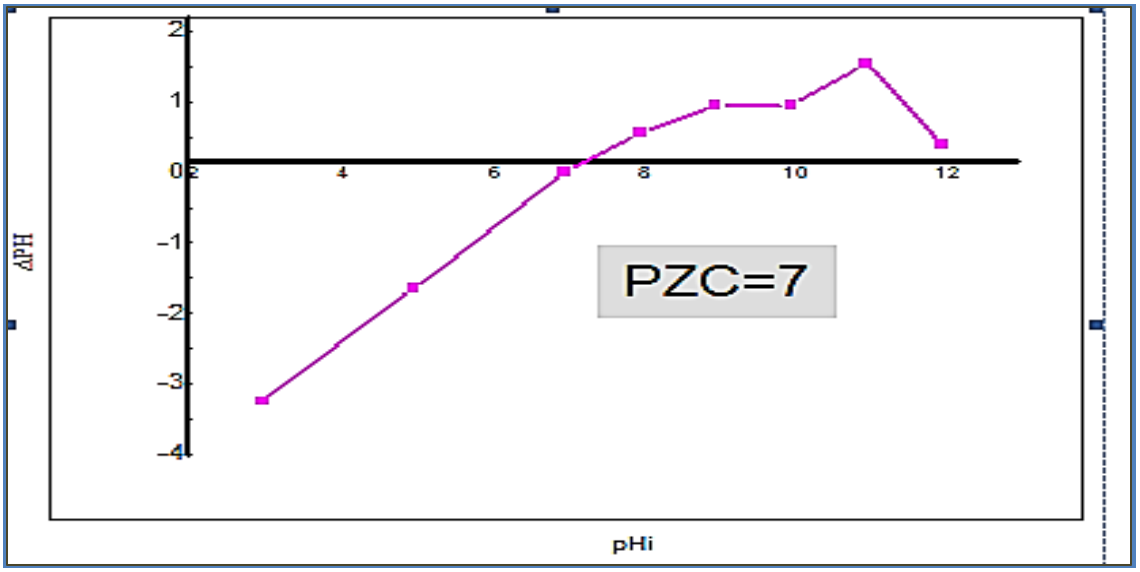

Appendix 4 : Point of zero charge of Cu-ZnO nanoparticles

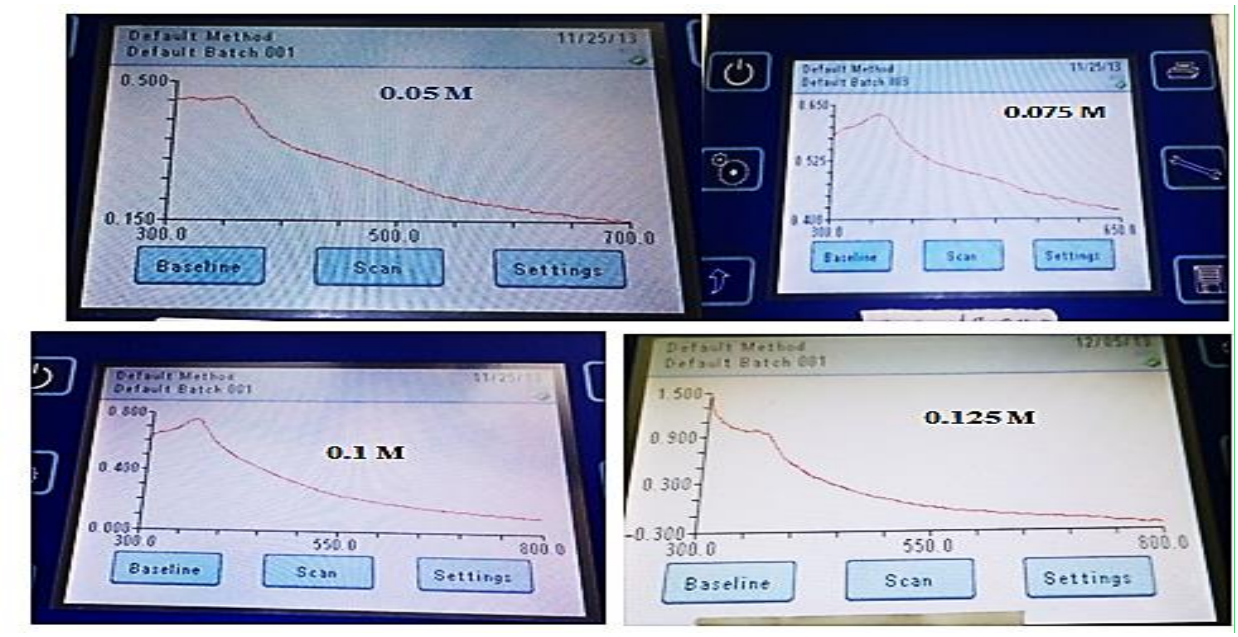

Appendix 5 : UV–Vis absorption spectra of the synthesized zinc oxide nanoparticles with concentration of precursor salt solution

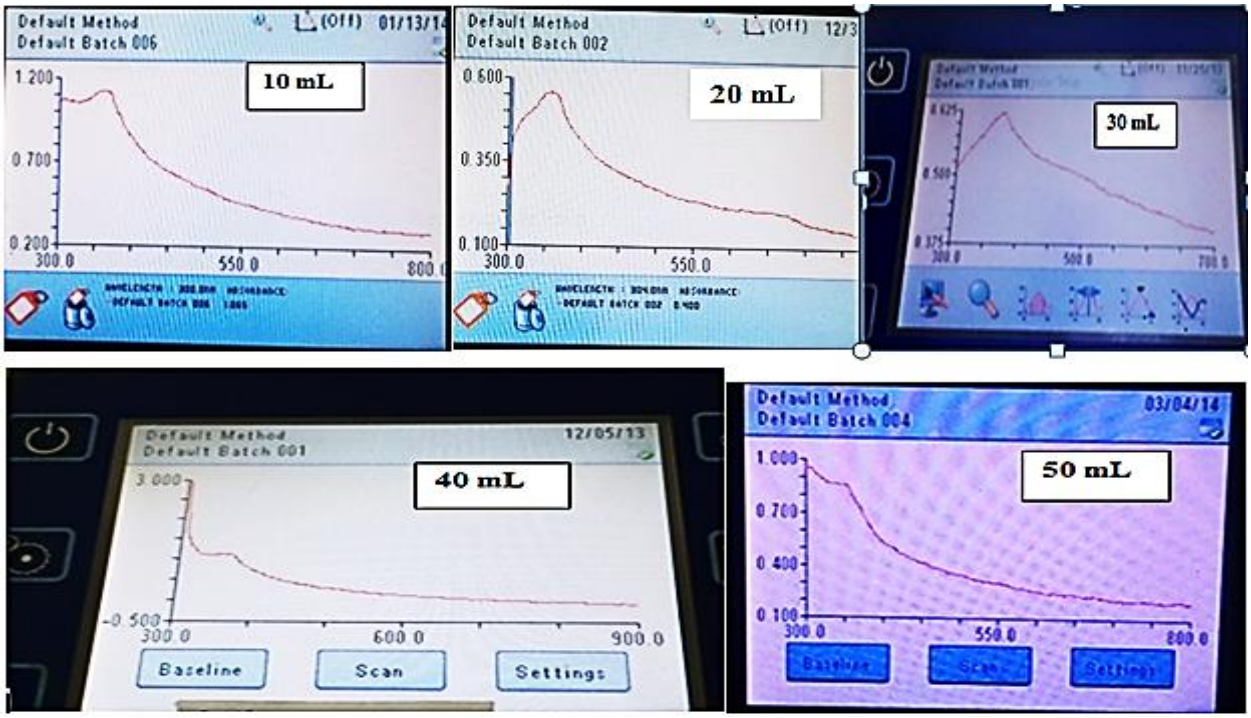

Appendix 6: UV–Vis absorption spectra of the synthesized zinc oxide nanoparticles with different volume of plant extract.

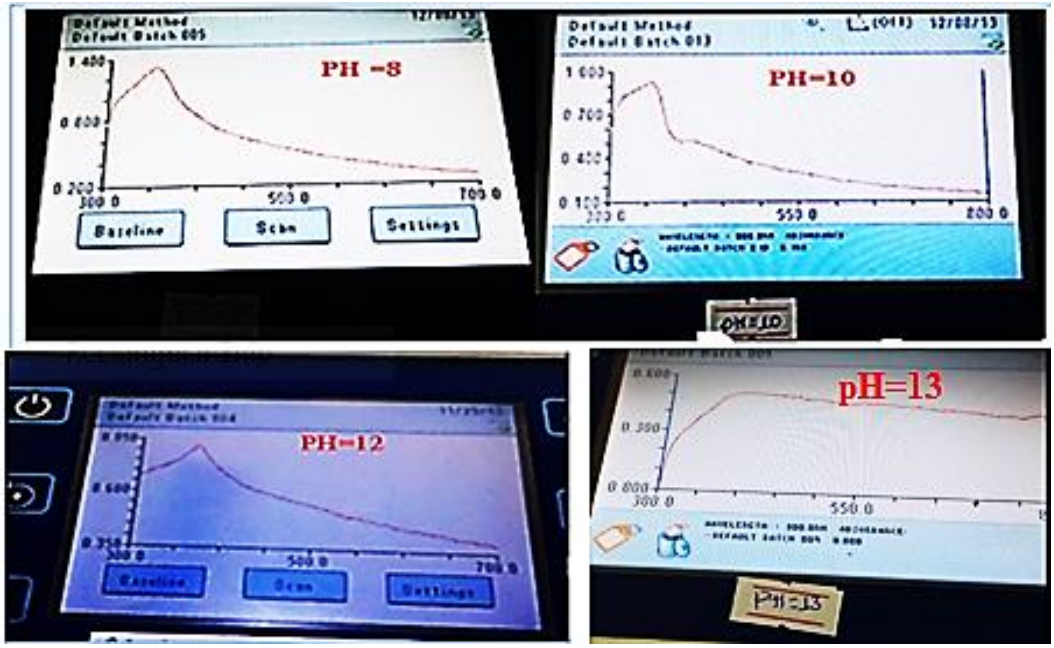

Appendix 7: UV–Vis absorption spectra of the synthesized zinc oxide nanoparticles at pH 8,10, 12 and 13

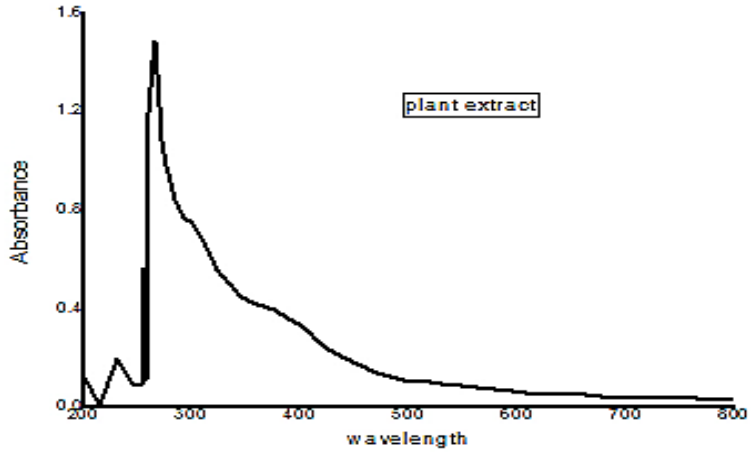

Appendix 8: UV-Vis absorbance of *Aloe vera* leaf extract